Cretaceous Research 49 (2014) 1–20

Contents lists available at ScienceDirect

Cretaceous Research

journal homepage: www.elsevier.com/locate/CretRes

Late Maastrichtian–early Danian high-stress environments and delayed recovery linked to Deccan volcanism

Jahnavi Punekar [a,*], Gerta Keller [a], Hassan Khozyem [b,1], Carl Hamming [a], Thierry Adatte [b,1], Abdel Aziz Tantawy [c], Jorge E. Spangenberg [b,1]

[a] Geosciences, Princeton University, Princeton, NJ 08540, USA
[b] Institute of Earth Sciences, University of Lausanne, 1015 Lausanne, Switzerland
[c] Department of Geology, Faculty of Science, Aswan University, Aswan 81528, Egypt

ARTICLE INFO

Article history:
Received 23 April 2013
Accepted in revised form 20 January 2014
Available online xxx

Keywords:
Deccan volcanism
KPB mass extinction
Delayed recovery
Guembelitria blooms

ABSTRACT

Deccan volcanism occurred in three intense phases of relatively short duration: phase 1 spanning the paleomagnetic chron C30r/C30n boundary (planktic foraminiferal CF4), phase 2 in the latest Maastrichtian C29r (zones CF1–CF2), and phase 3 in the early Danian C29n (P1b). This study explores the nature of paleoenvironmental changes correlative with the three volcanic phases in central Egypt and the Sinai based on planktic foraminifers, stable carbon and oxygen isotopes.

Results show that high-stress assemblages dominated by *Guembelitria* blooms are prominent in, but not exclusive to, all three volcanic phases. These blooms are well known from the aftermath of this mass extinction in zones P0–P1a, the intertrappean interval between volcanic phases 2 and 3. *Guembelitria* blooms in CF4 (phase 1) are relatively minor (<45%) although they comprise a substantial component of the planktic foraminiferal assemblages. Maximum *Guembelitria* blooms (>80% of the total assemblage) are observed in CF1, which spans the last 160 ka of the Maastrichtian marked by rapid global climatic warming and cooling correlative with phase 2. Major *Guembelitria* blooms (50–75%) are also observed in P1b, which is marked by climate warming (Dan-C2 event) and a major negative carbon isotope excursion correlative with phase 3. This high-stress event precedes full marine biotic recovery after the mass extinction.

Published by Elsevier Ltd.

1. Introduction

A large meteorite impact and one of the world's largest volcanic eruptions, resulting in the Deccan Traps in India, occurred in the latest Maastrichtian, an interval leading up to the Cretaceous–Paleogene boundary (KPB, formerly known as Cretaceous–Tertiary boundary or KTB). Of these two catastrophes, the meteorite impact is popularly assumed to be the sole cause for the KPB mass extinction (Alvarez et al., 1980; Schulte et al., 2010). However, major climatic, environmental and faunal changes during the late Maastrichtian and early Danian rule out a single cause. Deccan volcanism has been proposed as likely long-term cause (McLean, 1985; Courtillot et al., 1986, 1988) but a direct link with the mass extinction remained elusive. Improved paleomagnetic and radiometric dating have identified three major phases of Deccan volcanism (Chenet et al., 2007, 2008). The initial phase 1 (67.5 ± 1 Ma, C30n/C30r) accounts for ~6% of Deccan eruptions, the main phase 2 (C29r below the KPB) accounts for 80% of the total lava pile, and the last phase 3 (onset at C29r/C29n boundary) accounts for 14%. The discovery of marine deposits in intertrappean sediments of the Krishna-Godavari Basin quarries and subsurface cores (Keller et al., 2008, 2011a, 2012), and in outcrops of central India (Madhya Pradesh) (Keller et al., 2009a,b), have recently provided the first direct links between the KPB mass extinction and volcanic phase 2, as well as the delayed (>0.5 m.y.) post-KPB recovery and Deccan phase 3. These latter two volcanic phases, which account for 94% of the total volume of Deccan eruptions, are recognized as containing the world's largest and longest lava mega-flows >1000 km across India and out into the Bay of Bengal (Keller et al., 2008; Self et al., 2008).

The sheer volume of CO_2, SO_2 and Cl_2 associated with these volcanic eruptions suggest that Deccan volcanism had the potential to cause serious global environmental destruction (Self et al., 2005, 2008; Chenet et al., 2009). This is evident in intertrappean sediments between the C29r lava mega-flows of the Krishna-Godavari

* Corresponding author.
E-mail address: jpunekar@princeton.edu (J. Punekar).
[1] Current address: Department of Geology, Faculty of Science, Aswan University, Aswan 81528, Egypt.

0195-6671/$ – see front matter Published by Elsevier Ltd.
http://dx.doi.org/10.1016/j.cretres.2014.01.002

Basin (SE India) where the mass extinction is rapid and ends with the last phase 2 mega-flows at the KPB (Keller et al., 2011a, 2012). In Meghalaya (NE India) located ~800 km from the main Deccan province, blooms of the disaster opportunist *Guembelitria cretacea* dominate (>95%) in phase 2 with only rare Maastrichtian species present and all go extinct at the KPB, which is also marked by a large (12 ppb) Ir anomaly and negative $\delta^{13}C$ excursion (Gertsch et al., 2011). These observations now permit the evaluation of faunal assemblages and particularly *Guembelitria* blooms correlative with Deccan volcanism on a global basis. For example, *Guembelitria* blooms have previously been observed from the Middle East during the late Maastrichtian (zones CF1–CF2 and CF4 and in the early Danian P1b, although the cause(s) for these stressed conditions remained unexplained (Keller and Benjamini, 1991; Abramovich et al., 1998; Keller, 2002).

The objective of this study is to test the hypothesis that high-stress planktic foraminiferal assemblages observed in late Maastrichtian and early Danian sequences are caused by climatic and environmental changes that resulted directly from the main phases of Deccan volcanic eruptions in India. We chose central Egypt and the Sinai as test cases because of their proximity to the paleolatitude of India and the Reunion hotspot that resulted in the Deccan volcanic province (Fig. 1A), and because of the previously observed enigmatic *Guembelitria* blooms in the late Maastrichtian and early Danian in Israel (e.g., Keller and Benjamini, 1991; Abramovich et al., 1998). Three sections were chosen from the Central Eastern Desert (Wadi Hamama, Gebel Qreiya) and the Sinai (Wadi Nukhul, Fig. 1B). The fauna is relatively well-preserved and spans late Maastrichtian through the early Danian. Investigations concentrated on: (1) biostratigraphy, (2) faunal turnover, (3) *Guembelitria* blooms, (4) carbon and oxygen isotope stratigraphy, (5) correlation of *Guembelitria* blooms with Deccan volcanism, and 6) potential causes of biologic stress.

2. Geologic setting

Gebel Qreiya and Wadi Hamama are located in the central eastern desert of Egypt (26°21′N 33°01′E, Fig. 1B) at the southern tip of the Wadi Qena. Gebel Qreiya is 50 km northeast of Qena city and 18 km north of the Km53 marker on the Qena-Safaga road, whereas Wadi Hamama is ~28 km south of Gebel Qreiya and 10 km south of the Km44 marker on the Qena-Safaga road (26°18′N 33°02′E). During the late Maastrichtian and early Paleocene deposition occurred in a middle shelf (~100–200 m) environment marked by sea-level fluctuations and erosion (Said, 1961; Luger, 1988; Keller, 2002; Keller et al., 2002; Tantawy, 2003). Wadi Nukhul is located in the southwestern Sinai about 6 km south of Abu Zenima City, on the eastern side of the Gulf of Suez (29°01′N 33°15′E, Fig. 1). Sedimentation occurred in an outer shelf environment at a paleodepth of >200 m.

3. Lithology

At Gebel Qreiya and Wadi Hamama, the Dakhla Formation spans the upper Maastrichtian and lower Danian (Abdel Razik, 1972; Soliman et al., 1986), which was sampled and analyzed in a 24 m interval at the former (Fig. 2) and 22 m in the latter (Fig. 3). For Gebel Qreiya, the biostratigraphy (planktic foraminifera and nannofossils), sedimentology, mineralogy and stable isotopes of the upper 14 m were previously published (Keller, 2002; Keller et al., 2002; Tantawy, 2003) and only a brief summary is given here. This study added a 10 m interval at the bottom of the section for a more complete upper Maastrichtian record. The nannofossil and planktic foraminiferal biostratigraphy as well as the faunal and floral turnovers are similar in both sections (Tantawy, 2003).

At Gebel Qrieya, the basal 9 m consist of monotonous gray marly shale devoid of macrofossils (Fig. 2); this interval was not collected at Hamama. The gray shale grades into darker gray marly shale with abundant *Pecten farafrensis* shell fragments at Qreiya, though the equivalent interval at Wadi Hamama is devoid of macrofossils (Fig. 3). The *Pecten*-rich interval grades into monotonous marly shale with rare *P. farafrensis* and ends abruptly at disconformities ~1.8 m and 3 m below the KPB, as defined by the extinction of Maastrichtian and first appearance of Danian planktic foraminifers, at Gebel Qreiya and Wadi Hamam, respectively. Marly shale devoid of macrofossils overlies the disconformity and ends at another disconformity at the KPB in both sections (Fig. 3). At Qreiya, the KPB erosional surface overlies a 10-cm-thick bioturbated, fossiliferous marly shale (Fig. 2). Above this hiatus is a 1-cm-thick red clay layer devoid of calcareous microfossils, but enriched with gypsum and a 5.4 ppb Ir anomaly marks this KPB unconformity (Keller et al., 2002; Tantawy, 2003). In contrast, there is no marked erosional

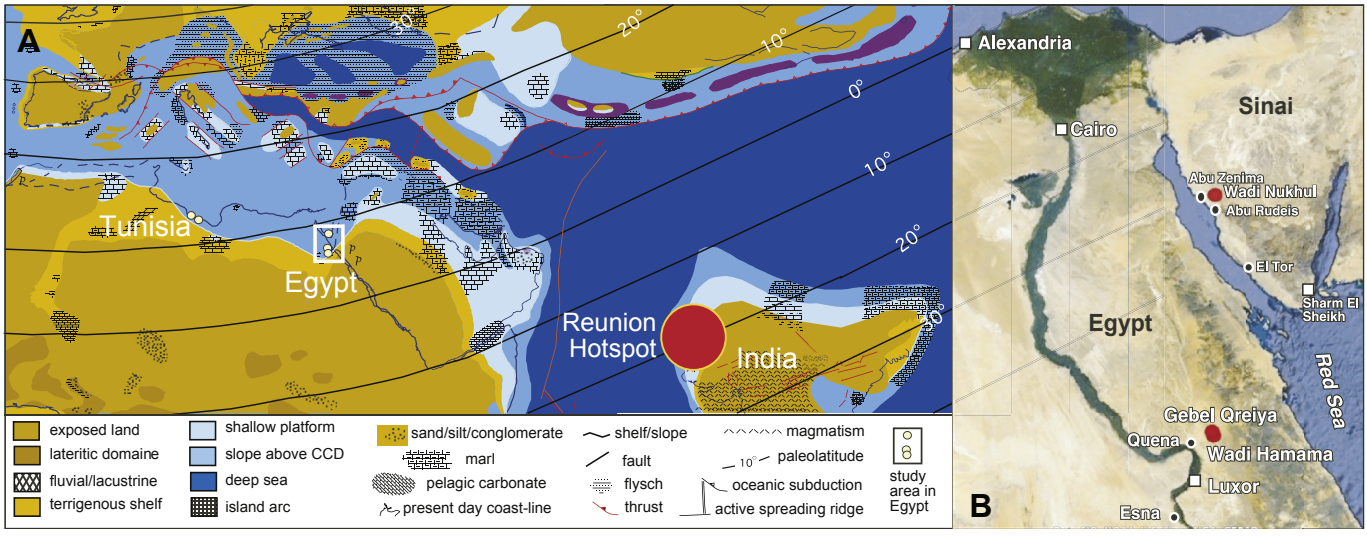

Fig. 1. (A) Paleogeography of Tethys, India and Reunion hotspot during the Cretaceous–Tertiary transition, modified after Dercourt et al. (1993); (B) Google Earth image showing the present day location of the studied sections in central Egypt and Sinai.

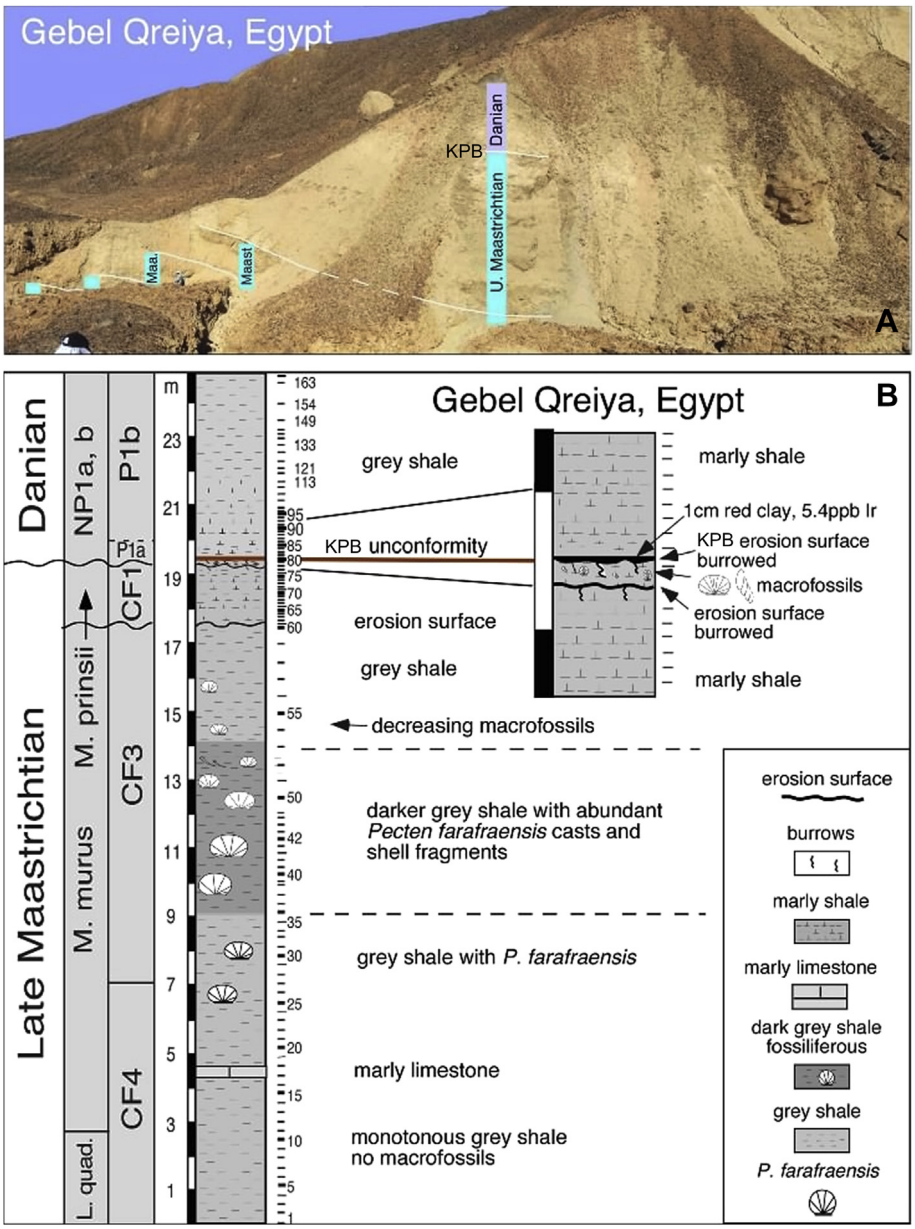

Fig. 2. (A) Gebel Qreiya, Egypt, with Maastrichtian to early Paleocene sequence. (B) Lithology and description of the interval analyzed.

surface or red layer observed at the KPB at Wadi Hamama (Fig. 3). At Qreiya and Hamama, a <0.5-m-thick, fissile, dark-gray shale overlies the red layer and contains an earliest Danian (P1a) faunal assemblages. Above this interval, gray marly shale marks sedimentation in the early Danian.

Wadi Nukhul contains one of the most continuous sedimentary sequences across the Cretaceous–Tertiary and Paleocene–Eocene transitions in Egypt (Fig. 4A). Most of the Maastrichtian consists of the Sudr Formation, which is characterized by white chalk intercalated with thin lamina of yellow calcareous shale. The contact between the Sudr Formation and the overlying Dakhla Formation is marked by a change to gray and yellow marly limestone at the top of a cliff. The lower part of the Dakhla Formation consists of an increasingly bioturbated, marly limestone with burrows infilled with gray shale (Fig. 4B, C). Fissile marly limestone grades into silty marl and shale with a gypsum layer at the top that marks the KPB unconformity. Above the unconformity yellow-gray marls are intercalated with ferruginous brown-red claystone with gypsum seams (samples Nua-112–116, Fig. 4B, A and B). The overlying Danian sediments consist of argillaceous limestone grading into gray calcareous shale (0.8 m thick). Above this interval is a prominent 5-cm-thick, red-brown ferruginous claystone with gypsum seams. The overlying calcareous shale is 1.4 m thick and multicolored (gray, brown, black, green, yellow) interrupted by two thin silty claystone layers (Fig. 4B).

4. Material and methods

For all three sections analyzed, samples were collected at 10–30 cm intervals and at closer spacing (~5 cm) across the KPB. In the laboratory, samples were crushed into small fragments and left overnight in 3% hydrogen peroxide solution to oxidize organic carbon. After disaggregation of sediment particles, the samples were washed through >63 μm and >36 μm sieves to obtain clean

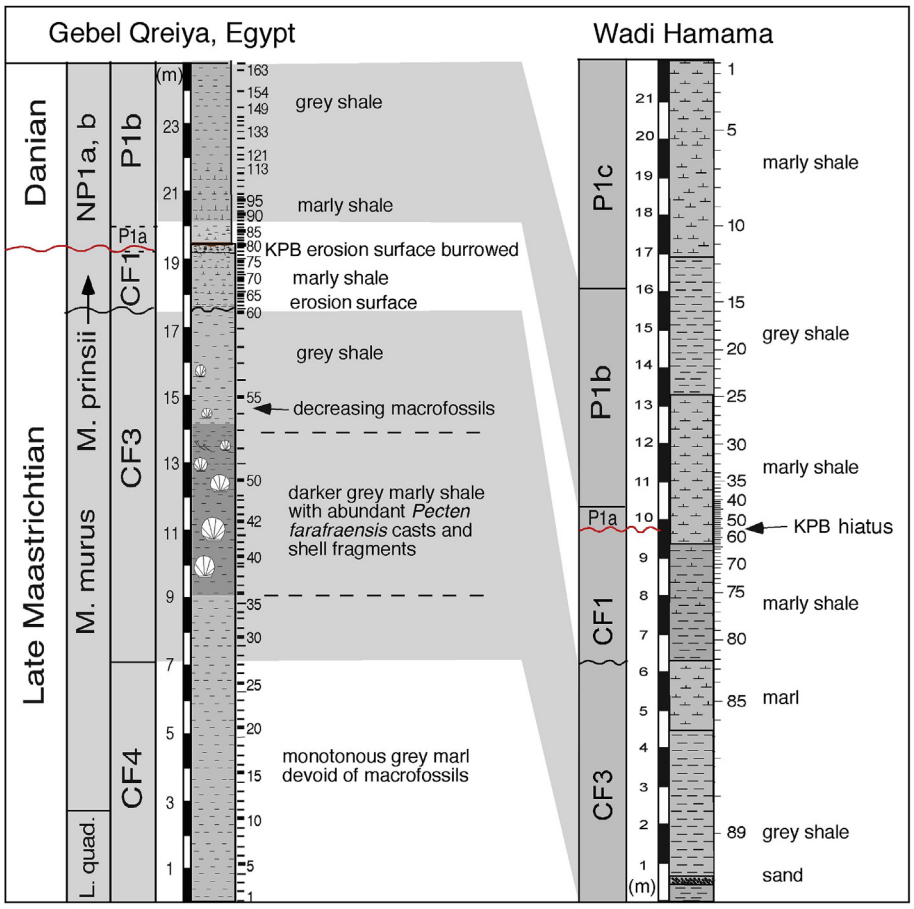

Fig. 3. Lithology and description of the Maastrichtian to early Paleocene sequence at Wadi Hamama compared with Gebel Qreiya, Egypt.

foraminiferal sample residues (Keller et al., 1995). Complete removal of clay is important to avoid clump formation upon drying. Washed residues were oven dried at 50 °C. Foraminifers from Maastrichtian limestone and marly limestone of the Wadi Nukhul section are difficult to free from adhering sediments even after boiling with $NaHCO_3$ and ultrasonic treatment; no reliable quantitative data could be obtained for these samples. Thin section analysis is not suitable for quantitative faunal studies because species identification is limited to a small number of specimens with species-specific characteristic cross sections.

To obtain a statistical representation of the species population, each sample was split with an Otto micro-splitter to obtain approximately 300 specimens from the >63 μm size fraction. Planktic foraminifers were picked from each split, sorted and mounted on micro-slides and identified. The entire remaining sample residue was thoroughly searched for rare index species for biostratigraphy, but not counted as part of the quantitative faunal split. Identification of species is based on standard taxonomic concepts (e.g., Robaszynski et al., 1983–84; Nederbragt, 1991; Olsson et al., 1999). Some of the typical species are illustrated in Plates 1–4.

Stable carbon and oxygen isotope analyses were performed on reasonably well-preserved tests of monospecific planktic and benthic foraminiferal species for samples from Gebel Qreiya consistent with the dataset of Keller et al. (2002). At Wadi Hamama and Wadi Nukhul bulk rock samples were analyzed due to poor foraminiferal preservation. These analyses were conducted at the Earth Sciences Institute (ISTE) of the University of Lausanne, Switzerland, using a Thermo Fisher GasBench II preparation device interfaced with a Thermo Fisher Delta Plus XL continuous flow isotope ratio mass spectrometer. The stable carbon and oxygen isotope ratios are reported in the delta (δ) notation as the per mil (‰) deviation relative to the Vienna Pee Dee belemnite standard (VPDB). The reproducibility was better than ±0.05‰ for $\delta^{13}C$ and ±0.1‰ for $\delta^{18}O$.

5. Biostratigraphy

The Cretaceous foraminiferal (CF) biozonation of Li and Keller (1998a) and Danian biozonation of Keller et al. (1995, 2002) are applied in this study (Fig. 5). Biozone ages are calculated based on the paleomagnetic time scales of Cande and Kent (1995) and Gradstein et al. (2004). Previous studies recognized most late Maastrichtian to early Danian planktic foraminiferal and nannofossil biozones at Gebel Qreiya, Wadi Hamama and Wadi Nukhul (Keller, 2002; Keller et al., 2002; Tantawy, 2003).

Zone CF4 (67–68.4 Ma): This zone spans the interval between the first occurrences (FO) of *Racemiguembelina fructicosa* and *Pseudoguembelina hariaensis* (Fig. 5). CF4 is tentatively identified in the basal 7 m of the Gebel Qreiya section based on the presence of rare *R. fructicosa* and absence of *P. hariaensis* (Fig. 6). The faunal assemblage is dominated by *Heterohelix navarroensis*, *H. planata* and *H. globulosa*, *H. costulata* and *H. costellifera* (Plate 1, 5–6). *Guembelitria cretacea* (Plate 4, 12) shows two abundance maxima at 1.5 m and 6–7 m from the base. *Globotruncana bulloides* and *Rosita fornicata* disappear after the first *G. cretacea* peak (Fig. 6). *Rosita plummerae* and *R. plicata* last occur before the second *G. cretacea* peak and *Archaeoglobigerina cretacea*, *A. blowi* and *G. wiedenmayeri*

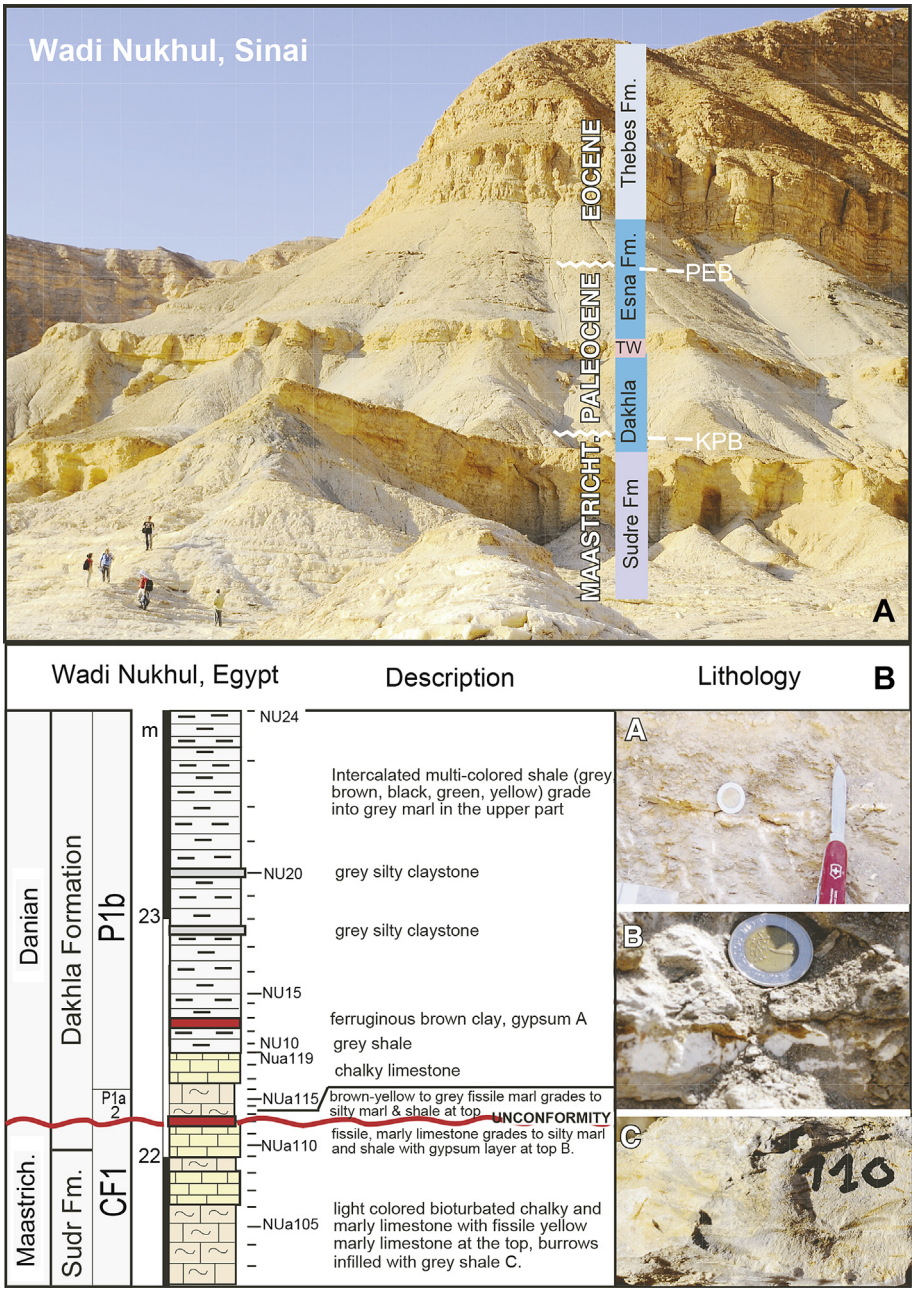

Fig. 4. (A) Maastrichtian through Paleogene sequence at Wadi Nukhul, Egypt. (B) Lithology and description of the interval analyzed.

disappear coincident with this *Guembelitria* peak. The disappearance of *G. bulloides*, *R. plummerae* and *R. fornicata* was previously reported from CF4 in DSDP 525A and Madagascar (Li and Keller, 1998a; Abramovich et al., 2002).

Zone CF3 (65.8–67 Ma): This zone spans the interval from the FO of *Pseudoguembelina hariaensis* (Plate 1, 4) to the last occurrence (LO) of *Gansserina gansseri* (Fig. 5). At Gebel Qreiya, CF3 spans 10.5 m (7–17.5 m, Fig. 6). *Guembelitria* blooms dominate faunal assemblages by 60% between 9.3–10.8 m and 11.8–13.3 m (peaks 3, 4). Near the top of CF3, *Guembelitria* blooms dominate assemblages by 80–90% (peak 5, Fig. 6). At the same time, species richness drops 19% (from 47 to 38 species). Heterohelicids continue to be the second-most dominant group in the assemblage, but decrease in abundance during *G. cretacea* blooms. A hiatus marks the top of CF3 with CF2 and an unknown interval of CF3 is missing.

At Wadi Hamama, CF3 marks the base of the section (1.5–4.5 m), which is dominated by *Guembelitria* blooms (60%, Fig. 7). Heterohelicids are common and globotruncanids very rare (Plate 2). *Guembelitria* blooms abruptly end at the lithologic change from gray shale to marl marking a hiatus between CF3 and CF1 similar to Gebel Qreiya.

Zone CF2 (65.7–65.8 Ma): This zone is defined by the interval between the LO of *Gansserina gansseri* and FO of *Plummerita hantkeninoides* (Fig. 5). At Gebel Qreiya and Wadi Hamama, the co-occurrence of these index species indicates a hiatus (Figs. 6 and 7) with at least CF2 missing (~150 ka based on Cande and Kent (1995) or 120 ka based on Gradstein et al. (2004), Fig. 5) and probably part of CF3. CF2 is present in the Negev sections of Israel, which were deposited in a deeper outer shelf to upper bathyal (300–500 m) environment (Adatte et al., 2005).

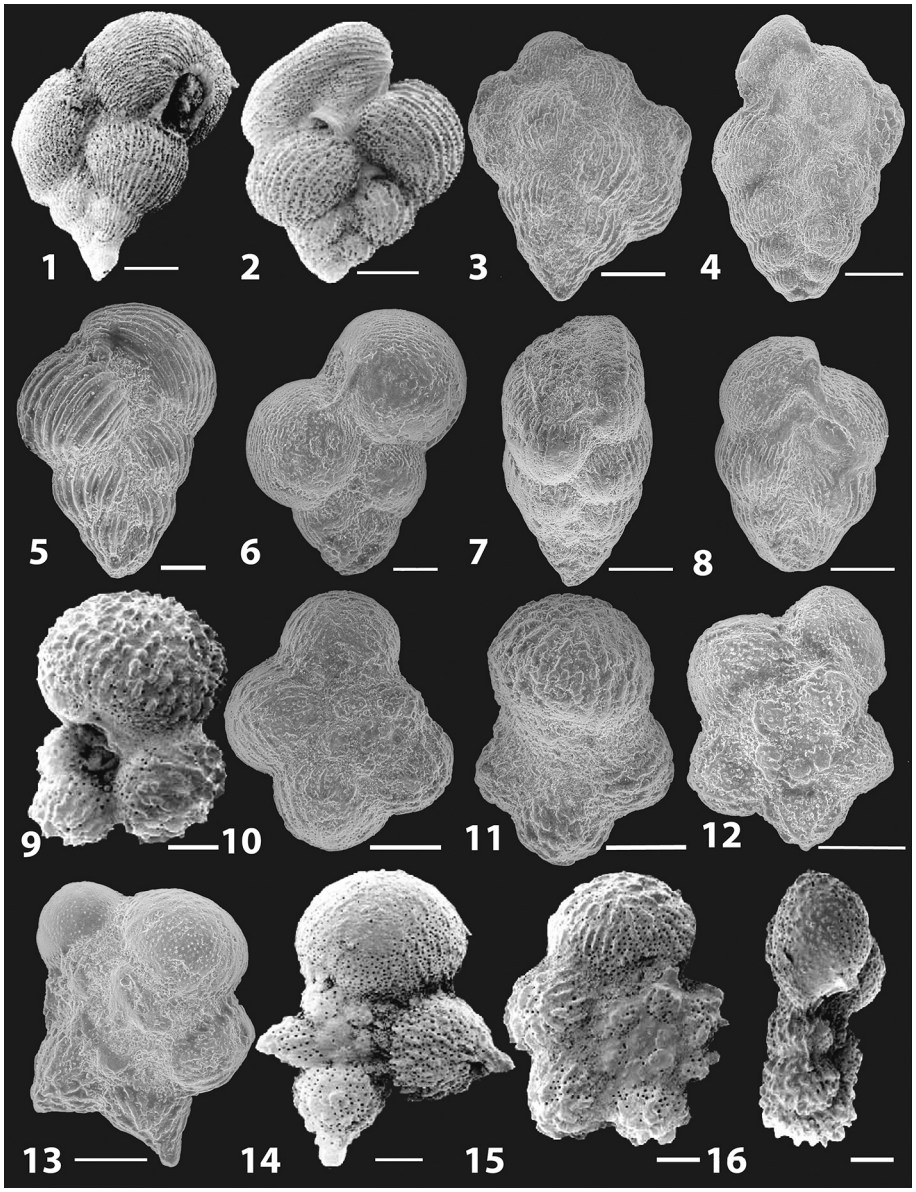

Plate 1. Maastrichtian planktic foraminifera from Gebel Qreiya (SEM images from Keller, 2002) and Wadi Nukhul, Egypt, scale bar = 50 μm.
1. *Planoglobulina carseyae* (Plummer), Gebel Qreiya.
2. *Pseudoguembelina palpebra* (Brönniman and Brown), Gebel Qreiya.
3. *Planoglobulina brazoensis* (Martin), Wadi Nukhul.
4. *Pseudoguembelina hariaensis* (Nederbragt), Wadi Nukhul.
5. *Pseudoguembelina costulata* (Cushman), Wadi Nukhul.
6. *Heterohelix globulosa* (Ehrenberg), Wadi Nukhul.
7. *Pseudotextularia elegans* (Rzehak), Wadi Nukhul.
8. *Heterohelix labellosa* (Nederbragt), Wadi Nukhul.
9. *Rugoglobigerina macrocephala* (Brönniman), Gebel Qreiya.
10. *Rugoglobigerina rugosa* (Plummer), Wadi Nukhul.
11–13. *Rugoglobigerina rugosa–Plummerita hantkeninoides* intermediate morphologies, Wadi Nukhul.
14. *Plummerita hantkeninoides* (Brönniman), Gebel Qreiya.
15–16. *Trinitella scotti* (Brönniman), Wadi Nukhul.

Zone CF1 (65.5–65.7 Ma): The total range of the index species *P. hantkeninoides* defines CF1. At Gebel Qreiya, CF1 spans a 2-m interval below the KPB (17.5–19.5 m, Fig. 6) with *P. hantkeninoides* (Plate 1, 11–14) consistently present. The CF1 assemblage is considerably lower (~20–30%) in species richness compared with older Maastrichtian biozones. Globotruncanids (Plate 2) are very rare. Heterohelicids and *G. cretacea* alternate in dominating the assemblages. Two peaks of *G. cretacea* are observed within CF1 although the distribution is uncertain due to hiatuses at the top and bottom of the zone (Fig. 6).

At Wadi Hamama, CF1 spans about 5 m below the KPB, but, just as at Gebel Qreiya, this biozone is truncated by hiatuses at the top and bottom leaving the true distribution of *Guembelitria* peaks uncertain. However, similar to Qreiya *Guembelitria* blooms dominate various intervals (Fig. 7). Most globotruncanids (Plate 2) and rugoglobigerinids (Plate 1, 9–16) disappeared at or below the KPB and species diversity is very low.

At Wadi Nukhul (Sinai), less than 1 m of CF1 was analyzed qualitatively because species could not be freed from the

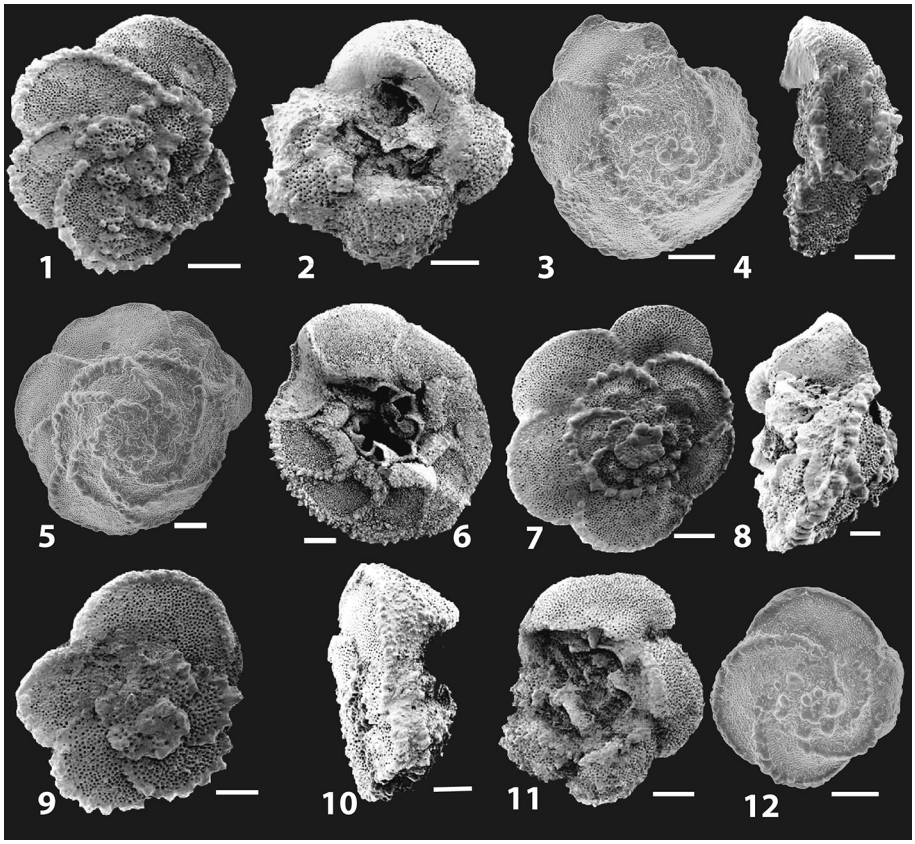

Plate 2. Maastrichtian planktic foraminifera from Gebel Qreiya (SEMS images from Keller, 2002) and Wadi Nukhul, Egypt, scale bar = 50 μm.
1–2. *Globotruncana rosetta* (Carsey), Gebel Qreiya.
3–4. *Globotruncanita conica* (White), spiral view – Wadi Nukhul, side view – Gebel Qreiya.
5–6. *Globotruncanita stuarti* (de Lapparent), spiral view – Wadi Nukhul, umbilical view – Gebel Qreiya.
7–8. *Globotruncana dupeublei* (Caron), Gebel Qreiya.
9–11. *Globotruncana aegyptiaca* (Nakkady), Gebel Qreiya.
12. *Globotruncanita pettersi* (Gandolfi), Wadi Nukhul.

limestones below this interval (Fig. 8). In the lower part of the analyzed interval, heterohelicids dominate especially *Heterohelix navarroensis*, *H. planata*, *H. globulosa*, *H. costulata* and *H. costellifera* whereas *G. cretacea* remains very low (<15%). In the 20 cm below the KPB, heterohelicids decrease and *G. cretacea* dominates (~50%). Species richness (25 species) reflects deposition in a middle- to outer-shelf environment (Keller and Abramovich, 2009). Globotruncanids and rugoglobigerinids are rare to few, although this is partly an artifact due to sample processing from limestones.

Definition of the KPB

The KPB is one of the easiest epoch boundaries to identify, whether based on lithologic changes in the field, geochemical analysis in the laboratory, or fossil content. A set of five KPB-identifying criteria, originally proposed by the ICS working group during 1980–1990s, have proven globally applicable and independently verifiable: (1) mass extinction of Cretaceous planktic foraminifera, (2) evolution of the first Danian species, (3) a KPB clay and red layer, (4) an Ir anomaly, and (5) a $\delta^{13}C$ shift (Keller, 2011). In central Egypt, the Sinai and Israel, the KPB transition is generally marked by erosion and condensed sedimentation of the earliest Danian and across the KPB (e.g., Keller and Benjamini, 1991; Keller, 2002; Keller et al., 2002; Tantawy, 2003). Nevertheless, the KT transition can be easily identified based on the defining criteria, except for the Ir anomaly, which may be concentrated at the hiatus due to redox concentrations.

Zone P0: This zone marks the base of the Danian in the interval between the mass extinction horizon and the first occurrence of *Parvularugoglobigerina eugubina* (Fig. 5). In complete KP sequences, P0 consists of a dark organic-rich KT clay layer with a 2–4 mm thin red oxidized layer enriched in iridium (Molina et al., 2006; Keller, 2011). Zone P0 is likely absent in Egyptian sections because of the KPB hiatus. At Gebel Qreiya, a thin dark clay and 1 cm red clay layer with a 5.4 ppb Ir anomaly overlies an erosional surface that truncates burrows of the underlying marl unit (Figs. 5 and 6, Keller, 2002). This rather small anomaly is likely linked to fluctuating redox conditions commonly associated with condensed sedimentation (e.g., Donovan et al., 1988; Bruns et al., 1997; Miller et al., 2010; Gertsch et al., 2011). At Wadi Hamama, no clay layer is present and the KPB hiatus is marked by a lithologic change from marly shale to marl (Fig. 7). At Wadi Nukhul, the KPB clay layer is also missing and the boundary is marked by an undulating erosional surface (Figs. 4 and 8). Reworked Cretaceous species are common in the overlying early Danian sediments.

***Zone P1a*:** This zone is identified by the total range of *Parvularugoglobigerina eugubina* (Plate 3, 13–14) and can be subdivided into P1a(1) and P1a(2) based on the FO of *Parasubbotina pseudobulloides* and/or *Subbotina triloculinoides* (Fig. 5, Plate 3, 5–6 and 1–2, respectively). At all three sections examined, P1a(2) directly overlies the KPB. This indicates that the earliest Danian P1a(1) and P0 are missing. Erosion of the earliest Danian is commonly observed in KPB sections throughout Egypt, Sinai and the Negev (Keller and

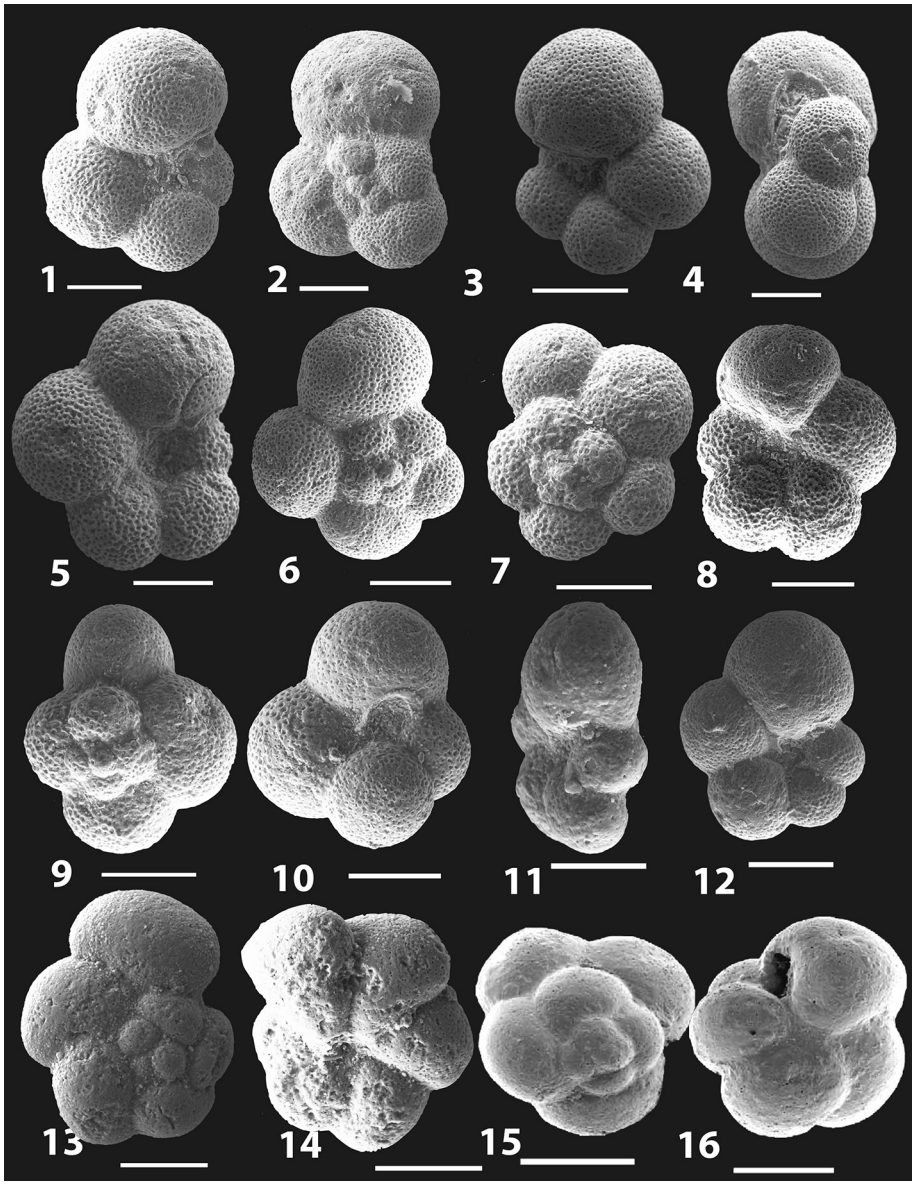

Plate 3. Danian planktic foraminifera from Gebel Qreiya (SEM images from Keller, 2002) and Wadi Nukhul, Egypt, scale bar = 100 μm.
1–2. *Subbotina triloculinoides* (Plummer), Wadi Nukhul.
3–4. *Parasubbotina varianta* (Subbotina), Wadi Nukhul.
5–6. *Parasubbotina pseudobulloides* (Plummer), Wadi Nukhul.
7–8. *Globigerina (Eoglobigerina) pentagona* (Morozova), Wadi Nukhul.
9–10. *Subbotina trivialis* (Subbotina), Wadi Nukhul.
11–12. *Globanomalina compressa* (Plummer), Wadi Nukhul.
13–14. *Parvularugoglobigerina eugubina* (Luterbacher and Premoli Silva), Wadi Nukhul.
15–16. *Parvularugoglobigerina extensa* (Blow), Gebel Qreiya.

Benjamini, 1991; Keller, 2002; Keller et al., 2002; Tantawy, 2003; Adatte et al., 2005), as well as Madagascar (Abramovich et al., 2002), South Atlantic (Li and Keller, 1998a), South America (Brazil, Argentina; Keller et al., 2007; Gertsch et al., 2013), Central America, (Keller et al., 2003, 2009b) and North Atlantic (Keller et al., 1993, 2013).

At Gebel Qreiya and Wadi Hamama, P1a(2) spans 50 cm of dark-gray marly shale, whereas at Wadi Nukhul only 15 cm is present (Figs. 6–8). *Parvularugoglobigerina* spp. dominate and show peak abundance ranging from 50% to 60% at Qreiya and Hamama and ~30% at Wadi Nukhul. *Guembelitria* is the other dominant group with maximum abundances of 75% at Qreiya, 50% at Wadi Nukhul and 30% at Hamama. The high variability in *Guembelitria* abundance between sections is mainly due to hiatuses and the resultant fragmented stratigraphic record of P1a with only part of P1a(2) present. *Chiloguembelina* spp. (Plate 4, 5, 8) and *Woodringina* spp. (Plate 4, 6–7) are present but not abundant.

A hiatus is identified at the top of P1a(2) in all three sections by the abrupt termination of abundant *Parvularogoglobigerina* and *Guembelitria* species followed by the abrupt dominance of *Globoconusa daubjergensis* (Plate 4, 3–4, 9–12). In more complete stratigraphic records termination and onset of these species is more gradual. Apart from *Guembelitria cretacea*, other Cretaceous survivor species (e.g., *Heterohelix globulosa*, *H. planata*, *H. navarroensis*, *P. costulata*, *Hedbergella monmouthensis*, *H. holmdelensis*) are identified based on their consistent presence and early Danian stable

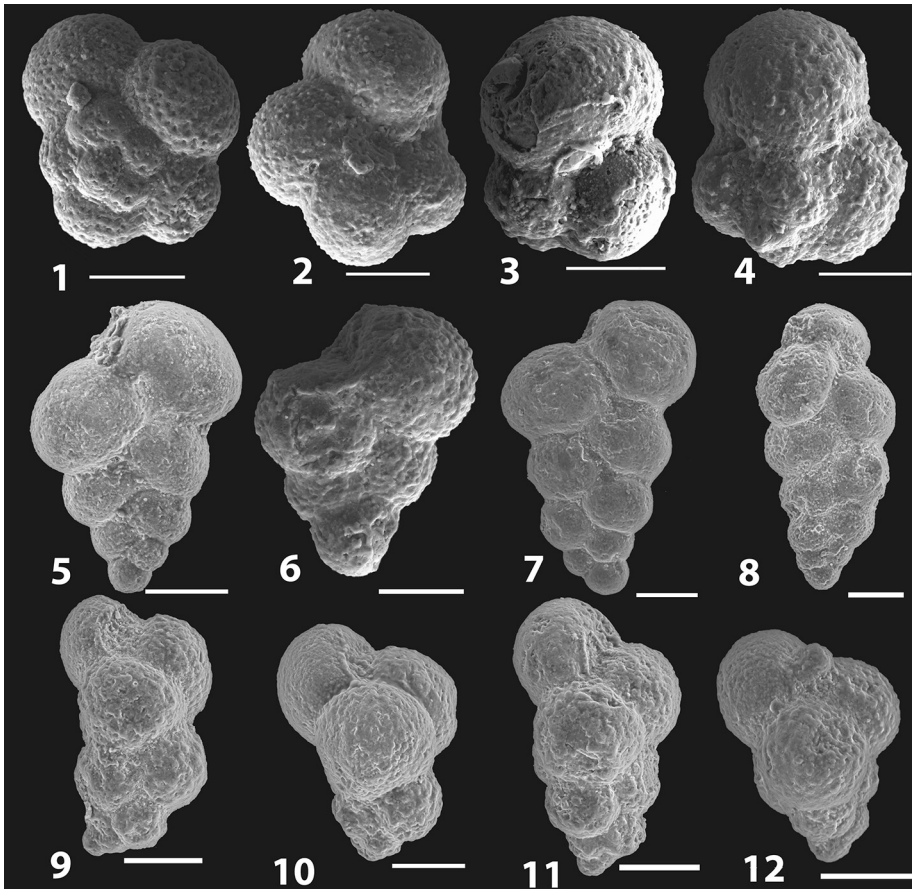

Plate 4. Danian planktic foraminifera from Wadi Nukhul, Egypt, scale bar = 50 μm.
1–2. *Eoglobigerina edita* (Subbotina).
3–4. *Globoconusa daubjergensis* (Brönnimann).
5. *Chiloguembelina midwayensis* (Cushman).
6. *Woodringina claytonensis* (Loeblich & Tappan).
7. *Woodringina hornerstownensis* (Olsson).
8. *Chiloguembelina morsei* (Kline).
9–10. *Guembelitria irregularis* (Morozova).
11. *Guembelitria danica* (Hofker).
12. *Guembelitria cretacea* (Cushman).

isotope signatures in P0 and P1a(1) in expanded and relatively complete KPB sequences (Barrera and Keller, 1990; Pardo and Keller, 2008). In Egypt and Israel where the early Danian is very incomplete with P0 and P1a(1) missing (Keller and Benjamini, 1991; Keller, 2002), the sporadically present Cretaceous survivor species in P1a(2) may be reworked.

Biozone P1b: This zone is the interval between LO of *P. eugubina* and FO of *Subbotina varianta* (Fig. 5). Zone P1b spans ~5 m at Gebel Qreiya, 6 m at Wadi Hamama and the top 1.5 m of Wadi Nukhul (Figs. 6–8). *Parvularugoglobigerina extensa* (Plate 3, 15–16) and *E. edita* (Plate 4, 1–2) disappear in the lower part of P1b. Most of the P1b species assemblages include survivors from P1a. *Praemurica pseudoinconstans* first appears in P1b, as also observed in the northwest Atlantic (Keller et al., 2013). Zone P1b is dominated by alternating abundances of *Guembelitria* spp. (*G. cretacea*, *G. trifolia*, *G. irregularis*; Plate 4, 9, 10, 12), *Globoconusa daubjergensis* (Plate 4, 3–4) and biserial species (*Woodringina hornerstownensis*, *W. claytonensis*, *Chiloguembelina morsei*; Plate 4, 5–8) suggesting a succession of variable high-stress environments (Figs. 6–8). At the top of P1b, *Guembelitria* spp. and *G. daubjergensis* decrease sharply and biserial species dominate in P1c. This changeover is a secondary marker for the P1b/P1c boundary.

Biozone P1c: Biozone P1c spans the interval between FO of *Subbotina varianta* (Plate 3, 3–4) and FO of *Praemurica trinidadensis*. Zone P1c was recovered at Wadi Hamama (Figs. 5 and 7). Most of the P1c species assemblage includes survivors of P1b. Biserial species dominate P1c and the overall species richness, species size and morphology increases in P1c.

6. Stable isotopes

Stable isotopes ($\delta^{13}C$ and $\delta^{18}O$) measured for all three sections from Egypt (Tables 1–3) are compared with data from Elles and El Kef, Tunisia, for the Maastrichtian–Danian interval (Keller and Lindinger, 1989; Stüben et al., 2003; Fig. 9). Although overall trends are similar for the late Maastrichtian, direct comparison is difficult due to the presence of hiatuses in Egypt.

The $\delta^{13}C$ record for the KPB transition at Gebel Qreiya was discussed in Keller et al. (2002). The key features include the decreasing surface-to-deep $\delta^{13}C$ trend with a reversal in planktic and benthic values in the upper part of CF3 (planktic $\delta^{13}C$ 0.2–0.8‰ lighter than benthic values, Fig. 9). In CF1, planktic values increase by 0.7‰ and decrease by 0.5‰ at the KPB hiatus. In contrast, at Elles, El Kef and globally planktic $\delta^{13}C$ values decrease 2–3‰ at the KPB. This difference is due to the hiatus in the Egyptian sections

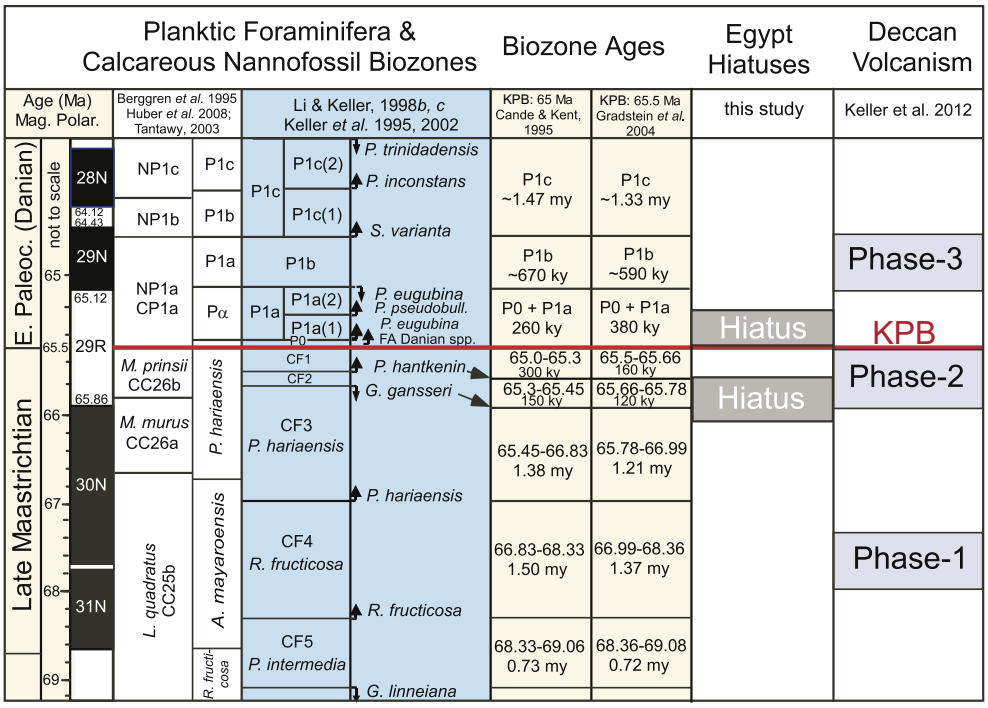

Fig. 5. Biozonation scheme applied in this study compared with alternative biozonations Ages for biozones are given for the time scales with the KPB at 65 Ma and at 65.5 Ma. Hiatuses observed in Egypt and ages of the three phases of Deccan volcanism are indicated.

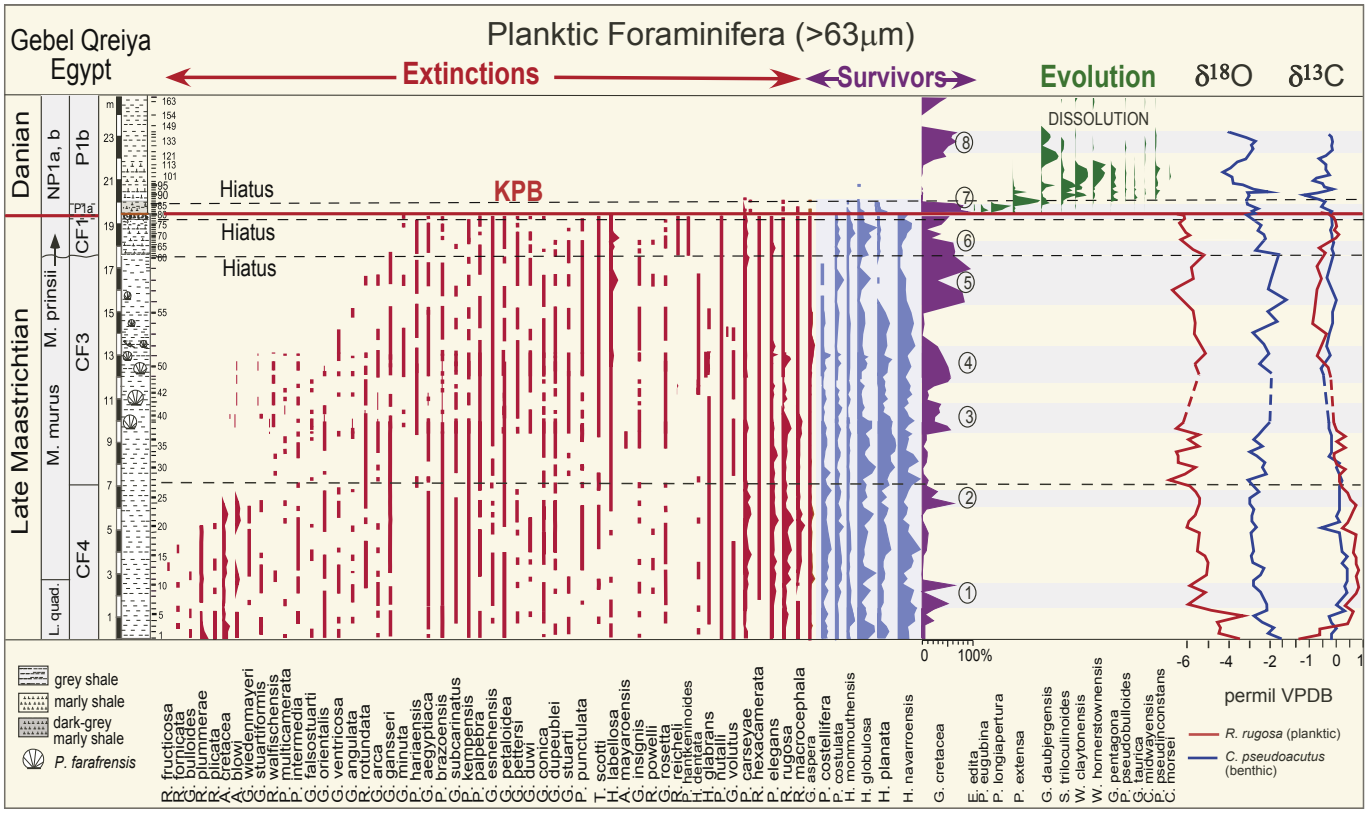

Fig. 6. Relative species abundances and turnover of planktic foraminifera (>63 μm) at Gebel Qreiya, Egypt. Note the gradual disappearances of species during the Late Maastrichtian culminating in the mass-extinction at the KPB, and the abundance peaks of *Guembelitria cretacea* that mark intervals of environmental stress. Nannofossil zones are based on Tantawy (2003).

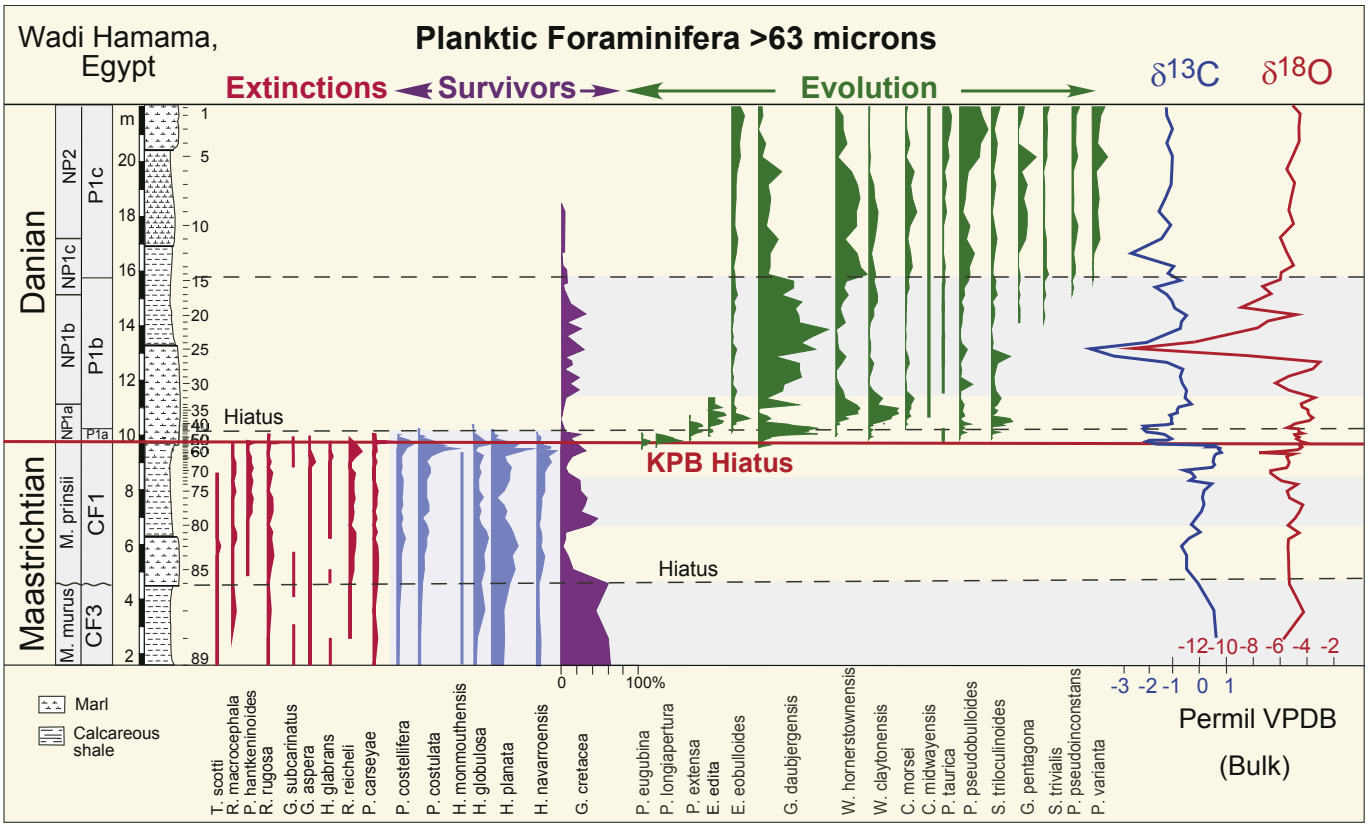

Fig. 7. Relative species abundances of planktic foraminifera (>63 μm) and $\delta^{13}C$ at Wadi Hamama, Egypt. High abundances of *Guembelitria cretacea* mark intervals high environmental stress. *Globoconusa daubjergensis* reflects high-stress in P1a(2) and P1b. Negative $\delta^{13}C$ excursions at the KPB and in P1b coincide with lithological changes and a KPB hiatus.

with the KPB interval missing. Benthic values gradually decrease in P1a(2) reach minimum values at the P1a(2)/P1b hiatus and fluctuate in P1b.

At Wadi Hamama and Wadi Nukhul, only bulk rock isotope analyses were performed because of poor preservation and insufficient quantity of early Danian planktic foraminifers for analysis. The late Maastrichtian $\delta^{13}C$ trend at Hamama is similar to the planktic $\delta^{13}C$ record of Gebel Qreiya with low values in CF3, more positive values in CF1 and a negative shift coincident with the KPB hiatus also observed at Wadi Nukhul (Fig. 9). Above the KPB, the earliest Danian is reduced to a small part of P1a(2) due to erosion. A 1‰ negative excursion at or near the P1a(2)/P1b hiatus is followed by partial recovery although $\delta^{13}C$ values remain about 2‰ below Maastrichtian values. At Wadi Hamama, a major negative excursion in P1b at a lithologic change from marl to dark shale occurs nearly 3 m above the hiatus. This interval was not recovered in the other Egypt or Tunisia localities, but was observed in Israel (Magaritz et al., 1992).

The $\delta^{18}O$ record at Gebel Qreiya shows a 2‰ negative shift in planktic $\delta^{18}O$ and 1.5‰ in benthic $\delta^{18}O$ values in the basal part of CF4. In CF3, increases in planktic and benthic $\delta^{18}O$ values (0.5–0.7‰) are similar to Elles. The entire CF2 and the lower part of CF1 are missing at Gebel Qreiya and Wadi Hamama (Figs. 6 and 7). All three localities show minimum $\delta^{18}O$ values at the top of CF3, although the CF3–CF1 hiatus prevents direct comparison with Elles. The top of CF1 at Qreiya and Hamama is reduced due to erosion at the KPB. Bulk isotopes at Wadi Hamama and Wadi Nukhul show the same trends as the planktic $\delta^{18}O$ values for Elles and Gebel Qreiya, although there are unique local short-term shifts (e.g., Danian of Wadi Hamama, about 3.5 m above the KPB, Fig. 9).

7. Discussion

7.1. Stable isotopes and diagenesis

At Gebel Qreiya, the planktic and benthic foraminifers (*R. rugosa*, *Cibicidoides pseudoacutus*) analyzed show diagenetic alteration of test calcite. This is evident in the foraminifer test wall structure with calcite overgrowth and the benthic tests commonly infilled with secondary calcite (Fig. 10). Recrystallization of foraminiferal tests tends to shift $\delta^{18}O$ values towards more positive values and $\delta^{13}C$ towards more negative values, thus biasing isotopic values towards cooler temperatures and lower productivity, although trends tend to be preserved (Schrag et al., 1995; Pearson et al., 2001).

Diagenetic effects can be observed in all three Egyptian sections analyzed. Maastrichtian $\delta^{18}O$ values for planktic foraminifers and bulk fine fraction carbonate vary between −4 and −6‰ in all sections, including Elles and El Kef, with an isolated larger excursion at Wadi Hamama. Therefore, the $\delta^{18}O$ values cannot be used for calculation of absolute temperature, although trends may be preserved. Very limited recrystallization can result in the observed negative values as indicated by the very low correlation coefficients of $\delta^{13}C$–$\delta^{18}O$ cross-plots (Fig. 11) and relatively constant diagenetic effects indicated by the surface-to-bottom water $\delta^{18}O$ gradient of 3–4‰. Burial diagenesis typically decreases this gradient (Schrag et al., 1995; Pearson et al., 2001; Stüben et al., 2003).

Climate trends in Tunisia and Egypt indicate warming in CF4 (Qreiya) followed by cooling in CF3 (Qreiya and Elles), which culminates in maximum cooling at the CF3/CF2 boundary coincident with a major sea-level regression and erosion in shelf areas (Li and Keller, 1998a; Keller et al., 2002). These climate signals also

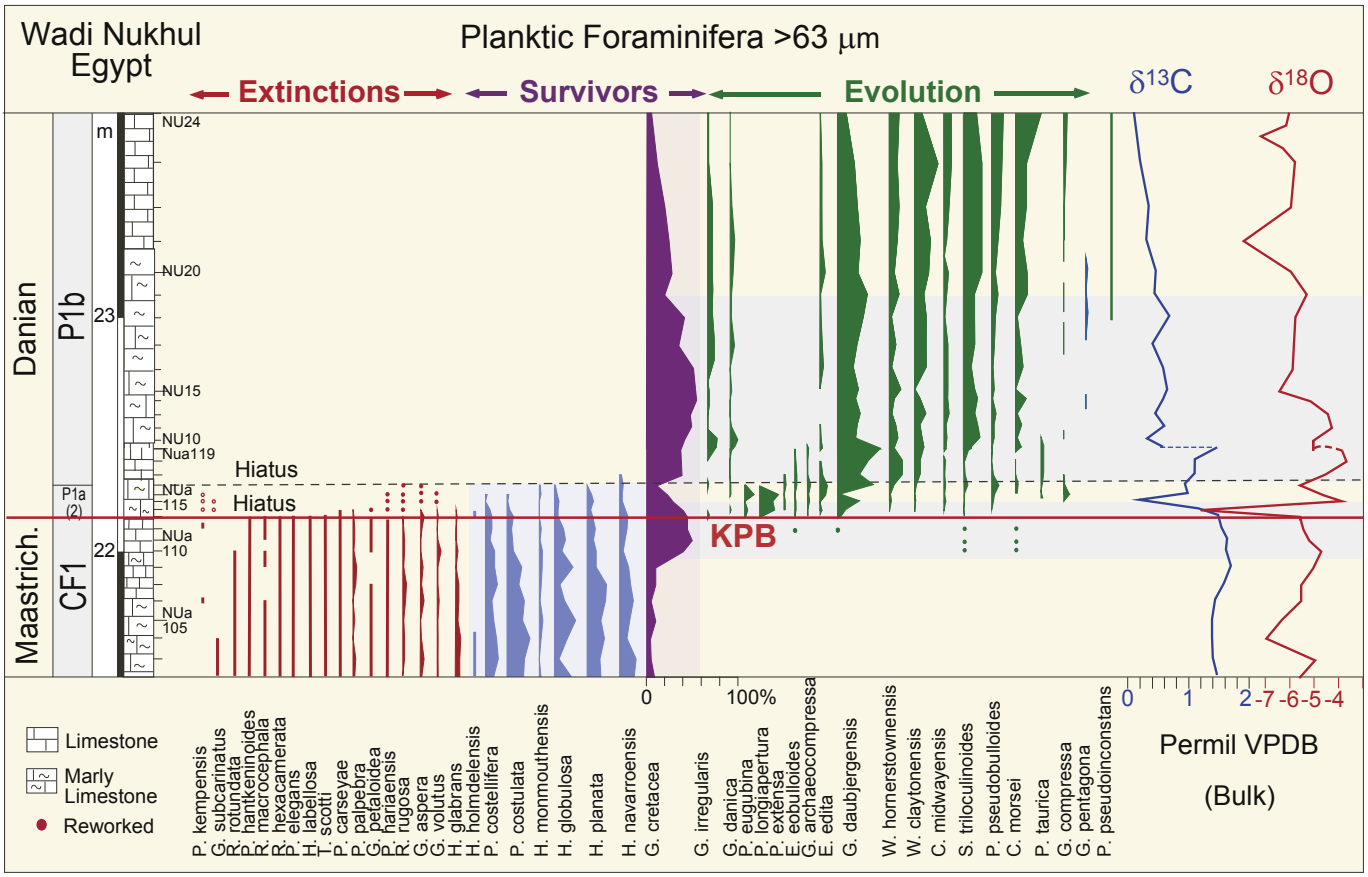

Fig. 8. Relative abundances of planktic foraminifera (>63 μm), oxygen and carbon isotopes at Wadi Nukhul, Sinai. Note the $\delta^{18}O$ excursion near the KPB hiatus is due to abundant reworked Cretaceous species in bulk sediments analyzed. $\delta^{13}C$ excursions are observed in the upper P1a(2) and lower part of P1b.

recorded in Madagascar, Israel, equatorial Pacific Sites 463, 1212, South Atlantic Site 525 and US interior (Li and Keller, 1998a; Abramovich et al., 2002, 2003, 2010; Nordt et al., 2003). At Elles, the expanded zones CF1–CF2 record shows several intervals of surface warming, including two in CF1 (Fig. 9, Stüben et al., 2003). At Qreiya, only a single warm interval is recorded in CF1 due to the KPB hiatus and similarly incomplete CF1–CF2 records are present at Wadi Hamama and Wadi Nukhul. The early Danian record in Egypt is also very incomplete with a hiatus between zones P1a/P1b, and another hiatus with the earliest Danian P1a(1) and P0 missing (~100 ka) along with the uppermost part of Maastrichtian CF1 (Fig. 5). In P1b, major negative $\delta^{18}O$ excursions are observed at lithologic changes that are partly due to diagenesis, but also record climate warming as indicated by blooms of *G. cretacea* and *G. daubjergensis* (Fig. 9). This warm interval may correspond to the early Danian Dan-C2 warm event near the top of C29r correlative with phase 3 Deccan volcanism (Quillévéré et al., 2008; Punekar et al., in press).

Some puzzling features in the oxygen and carbon isotope trends at Gebel Qreiya seem to have variable origins. For example, the reverse $\delta^{13}C$ gradient (more negative planktic than benthic values) can be explained by the relatively constant terrestrial ^{12}C influx and greater recrystallization of planktic tests due to their thinner and more porous wall structure (Keller et al., 2002; Stüben et al., 2003). Intervals of low $\delta^{13}C$ planktic values are correlative with a major reduction in large specialized species (thermocline dwellers), and assemblages dominated (75–90%) by the disaster opportunist *G. cretacea* or *H. globulosa* (Fig. 12). Keller et al. (2002) attributed these changes to the maximum cooling and sea-level regression in CF3–CF2 resulting in restricted circulation in central and southern Egypt. Alternatively, the low $\delta^{13}C$ values of Dissolved Inorganic Carbon (DIC) may be due to increased terrestrial weathering and detrital influx due to drawdown of higher atmospheric pCO_2 and/or low $\delta^{13}C$ of atmospheric CO_2 associated with surface ocean acidification (recorded in partially to completely dissolved foraminifer tests). All these phenomena and the global climate warming of Zones CF2–CF1 are consistent with large-scale Deccan volcanism as observed during the main phase 2.

7.2. Paleoenvironment inferred from planktic foraminifera

Species richness

Low species richness is a proxy for environmental stress because high-stress environments generally exclude specialized species due to changes in oxygen, nutrient, salinity and watermass stratification (Keller and Abramovich, 2009). However, during the late Maastrichtian the constant variation between 30 and 40 species in central Egypt provides little information on stress conditions. In contrast, cumulative species richness, which is based on the assumption that a species is present from its evolutionary first appearance to its extinction, provides an estimate of long-term evolutionary trends. At Gebel Qreiya, this index reveals a decreasing trend from a high of 60 species in CF4 to a low of 30 species at the KPB hiatus (Fig. 12). This decreasing trend parallels the surface productivity ($\delta^{13}C$), except that during the climate warming of CF1 species richness fails to recover as a likely response

Table 1
Gebel Qreiya, Egypt, carbon and oxygen stable isotope data (per mil. VPDB) for planktic (*Rugoglobigerina rugosa*) and benthic (*Cibicidoides pseudoacutus*) foraminifera.

Benthic			Planktic		
Sample	$\delta^{13}C$	$\delta^{18}O$	Sample	$\delta^{13}C$	$\delta^{18}O$
37	−1.73	−3.34	37	−3.43	−6.72
36	−2.37	−3.23	36	−3.67	−6.18
35	−0.3	−3.0	35	−0.1	−7.2
34	−0.3	−3.3	34	0.0	−7.5
33	−0.2	−3.6	33	0.3	−6.4
32	−0.2	−3.8	32	0.0	−6.9
31	−0.2	−3.4	31	0.3	−6.4
30	−0.2	−4.0	30	−0.1	−7.5
29	−0.3	−3.7	29	−0.1	−7.4
28	0.1	−3.3	28	0.0	−7.4
27	0.0	−3.4	27	0.3	−6.6
26	0.1	−3.2	26	0.1	−7.1
25	0.2	−4.1	25	0.1	−7.8
24	0.1	−3.8	24	0.2	−6.8
23	0.1	−3.6	23	0.4	−6.6
22	0.1	−4.0	22	0.5	−6.4
21	0.1	−4.0	21	0.7	−6.4
20	0.1	−3.8	20	0.6	−6.5
19	0.0	−3.9	19	0.5	−6.6
18	0.1	−3.9	18	0.4	−6.9
17	−0.6	−3.7	17	0.2	−7.0
16	0.1	−3.9	16	0.7	−6.4
15	0.2	−3.8	15	0.6	−6.5
14	0.3	−3.9	14	0.7	−6.2
13	0.2	−3.8	13	0.7	−6.0
12	0.4	−3.3	12	0.8	−14.2
11	0.4	−3.5	11	0.7	−6.1
10	0.4	−3.8	10	0.8	−6.9
9	0.3	−3.8	9	0.8	−6.8
8	0.4	−3.5	8	0.7	−6.2
7	0.0	−3.2	7	0.3	−6.9
6	0.3	−3.2	6	0.6	−5.8
5	−0.3	−3.7	5	−2.0	−4.3
4	−0.2	−3.4	4	0.4	−5.6
3	0.0	−2.7	3	−0.6	−5.4
2	−0.2	−3.1	2	−0.6	−5.5
1	−0.2	−2.4	1	−1.4	−4.5
48	−2.9	−4.9	48	−7.68	−9.34
47	−1.8	−3.6	47	−2.61	−7.78
46	−2.8	−4.1	46	−6.66	−7.96
45	−2.4	−3.4	45	−2.11	−7.51
44	−2.9	−4.0	44	−2.27	−7.80
43	−3.7	−3.9	43	−4.71	−7.73
42	−1.8	−3.0	42	−2.60	−7.24
41	−3.0	−3.7	41	−6.71	−7.19
40	−2.2	−3.8	40	−3.81	−7.29
39	−1.8	−3.6	39	−1.95	−7.10
38			38	−2.85	−7.09

to continued high-stress conditions. This relationship between stress conditions and non-recovery leading up to the KPB mass extinctions is still under investigation. Species abundance variations are another index of environmental stress because they are highly sensitive to changes in oxygen, salinity, temperature, nutrients and a host of still unknown other environmental parameters.

Large specialized species: intermediate or thermocline dwellers

We can group species based on stable isotope depth ranking into surface, subsurface mixed layer, intermediate or thermocline and deep-water dwellers based on oxygen and carbon isotope ranking of well-preserved specimens (Abramovich et al., 2003, 2010). Large ornate tropical and subtropical species, such as planoglobulinids, racemiguembelinids and globotruncanids (Plate 2), tend to be highly specialized (K-selected) species that

Table 2
Wadi Hamama, Egypt, bulk carbon and oxygen stable isotope data (per mil. VPDB).

Sample	$\delta^{13}C$	$\delta^{18}O$
S1	−1.31	−4.61
S2	−1.28	−4.01
S3	−1.06	−4.12
S4	−1.30	−4.13
S5	−1.08	−4.49
S6	−1.09	−4.94
S7	−1.12	−4.43
S8	−1.36	−4.69
S9	−1.60	−4.80
S10	−1.14	−4.48
S11	−1.49	−5.54
S12	−2.71	−5.04
S13	−1.02	−4.57
S14	−1.26	−5.42
S15	−0.74	−5.48
S16	−1.74	−6.87
S17	−1.31	−6.27
S18	−1.10	−7.20
S19	−0.98	−8.41
S20	−0.52	−4.34
S21	−0.72	−6.44
S22	−0.76	−7.20
S24	−2.08	−11.94
S25	−4.99	−16.44
S26	−3.57	−7.89
S27	−1.27	−2.56
S28	−0.65	−3.19
S29	−0.73	−4.80
S30	−0.64	−5.80
S31	−0.49	−2.88
S32	−0.53	−4.87
S33	−0.28	−3.93
S34	−0.82	−3.83
S35	−0.86	−3.40
S36	−0.85	−3.40
S37	−1.17	−3.34
S38	−1.09	−3.16
S39	−1.13	−3.30
S40	−1.08	−4.39
S41	−1.09	−4.66
S42	−1.31	−4.71
S44	−2.23	−4.97
S45	−2.14	−4.24
S46	−2.25	−4.28
S47	−2.10	−3.78
S48	−1.67	−4.41
S49	−1.42	−4.37
S50	−1.30	−4.24
S51	−1.12	−4.35
S52	−1.28	−4.11
S53	−1.97	−3.92
S54	−2.11	−3.57
S55	−1.69	−4.03
S56	0.55	−4.14
S57	0.43	−3.89
S58	0.73	−4.07
S59	0.84	−4.28
S60	0.78	−5.35
S61	0.91	−7.15
S62	0.74	−4.49
S63	0.67	−4.79
S64	0.67	−5.05
S66	0.59	−4.73
S67	0.57	−4.83
S68	0.63	−5.16
S69	0.54	−6.29
S70	−0.59	−6.25
S71	−0.31	−6.24
S72	−0.16	−5.80
S73	−0.36	−5.45
S74	0.52	−4.33
S75	0.23	−5.06
S76	0.15	−4.81

(*continued on next page*)

Table 2 (*continued*)

Sample	$\delta^{13}C$	$\delta^{18}O$
S77	0.21	−3.87
S78	0.09	−4.12
S79	−0.09	−4.40
S80	−0.29	−4.88
S81	0.05	−4.17
S82	−0.41	−4.80
S83	−0.71	−4.94
S84	−0.48	−4.80
S85	−0.47	−4.80
S86	−0.05	−4.73
S87	0.54	−3.79
S88	0.71	−5.31

require specific food sources, occupy narrow ecological niches and produce few offspring (Abramovich et al., 2003). At times of environmental stress, this large group of species (50% at Qreiya) is the first to disappear and their extinction is complete by the KPB (Keller, 2001). Globotruncanids are the largest and most diverse group of large, specialized species. They lived at intermediate or thermocline depths and include photosymbiotic species such as *Racemiguembelina* and *Contusotrunca* (Abramovich et al., 2010).

In central Egypt, globotruncanids in CF4 reached a maximum diversity of 25 species (42%) and peak abundance of 30%, although only 18 species are present in any given sample (Figs. 6 and 11). This ending phase for globotruncanids likely coincides with a time of maximum surface productivity, increased surface-to-deep gradient and climate warming as indicated by $\delta^{13}C$ and $\delta^{18}O$ respectively (Figs. 9 and 11). However, this coincidence requires further validation by other proxies. Near the top of CF4 and into CF3, globotruncanid diversity declined to 3–7 species and <10% abundance correlative with decreasing surface productivity to the level of benthic $\delta^{13}C$ values and climate warming. An increase in species richness in the lower part of CF3 to 12 species and ~20% abundance (9.7–10.1 m) correlates with a temporary increase in surface productivity and climate cooling. Thereafter, species richness dropped to 3–7 species totaling no more than 3% in relative abundance correlative with the inverse $\delta^{13}C$ surface-to-deep gradient (Fig. 12). A similar inverse gradient is observed at the base of the section. During the CF1 global warming globotruncanids briefly recovered to 10 species but relative abundance remained low up to their extinction at the KPB boundary. Earlier studies of the CF1 warm event documented decreased diversity and dwarfed species, including globotruncanids, pseudotextularids (e.g. *P. elegans*, Plate 1, 7) and pseudoguembelinids (e.g. Plate 1, 2, 4, 5) (Li and Keller, 1998a,b; Abramovich and Keller, 2003). These data suggest that globotruncanids and photosymbiotic forms thrived in a well-stratified oligotrophic water column (Abramovich et al., 2010).

Small morphologies: subsurface mixed layer

Subsurface mixed layer dwellers include a large group of relatively small species with simple morphologies and minor surface ornamentation, including heterohelicids, rugoglobigerinids, hedbergellids and globigerinelloidids (Abramovich et al., 2003, 2010). Their consistent high abundance in shallow water (compared to deeper marine environments) and only episodic increased abundance in deeper environments coupled with a disappearance of ornate specialized species suggests that these species can adapt to wide ecological niches and are likely more tolerant of fluctuations in environment and food sources (r-selected). Population dynamics of these species suggest that they multiply rapidly under conditions unstable for other species and dominate the assemblage, thus increasing chances of survival (Pardo and Keller, 2008; Keller and Abramovich, 2009). The small heterohelicids, including *Heterohelix globulosa*, *H. navarroensis* and *H. planata* (Figs. 6–8) are dominant in this group.

At Qreiya, the surface-mixed-layer group includes 10–13 species dominated by heterohelicids (70–90%) from CF4 to the base of CF3 (0–9 m), except for very short intervals of *Guembelitria* blooms (Fig. 12). In the middle and upper CF3, species richness reaches a maximum of 16 and gradually decreases to eight, correlative with decreasing population abundance from 60% to nearly zero prior to the CF3/CF1 hiatus. This decrease coincides with the inverse surface-to-deep gradient, common globigerinelloidids and rare globotruncanids. Abramovich et al. (2010) observed a similar species distribution in Israel and suggested mesotrophic conditions, whereas in oligotrophic open-marine conditions globotruncanids are more common and globigerinelloidids rare (e.g., DSDP site 525a, Li and Keller, 1998a; Tunisia, Abramovich and Keller, 2002). During the climate warming and high productivity of CF1 subsurface dwellers increased to 16 species with high population abundance (~90%) including 30% rugoglobigerinids (Fig. 12). A similar increase in rugoglobigerinids is observed in the Negev sections in zones CF1–CF2 (Abramovich et al., 2010).

Biserial morphologies

In oligotrophic environments, surface dwellers consist of a small group of biserial species that includes *Pseudoguembelina costulata*, *P. costellifera*, *P. palpebra* and *P. hariaensis* (Abramovich et al., 2003, 2010). These species are most abundant and characterized by

Table 3
Wadi Nukhul, Egypt, bulk carbon and oxygen stable isotope data (per mil. VPDB).

Sample	$\delta^{13}C$	$\delta^{18}O$
Nu-25	0.08	−6.04
Nu-24	0.21	−5.96
Nu-23	0.32	−6.26
Nu-22	0.46	−7.27
Nu-21	0.42	−6.28
Nu-20	0.58	−5.73
Nu-19	0.56	−5.90
Nu-18	0.80	−8.00
Nu-17	0.53	−5.91
Nu-16	0.70	−5.26
Nu-15	0.77	−5.74
Nu-13	0.57	−5.80
Nu-12	0.73	−6.39
Nu-11	0.43	−5.11
Nu-10	0.69	−4.40
Nu-9	0.63	−4.27
Nu-8	0.70	−5.12
Nua-119	1.58	−3.80
Nua-118	1.18	−3.67
Nua-117	1.12	−4.50
Nua-116	0.95	−5.57
Nua-115	1.10	−4.63
Nua-114	0.30	−3.75
Nua-113	1.27	−9.63
Nua-112	1.60	−5.56
Nua-111	1.66	−5.44
Nua-110	1.75	−5.23
Nua-109	1.74	−4.68
Nua-108	1.83	−5.07
Nua-107	1.69	−5.53
Nua-106	1.55	−5.54
Nua-105	1.49	−6.32
Nua-104	1.50	−6.97
Nua-103	1.56	−4.93
Nua-102	1.58	−5.61

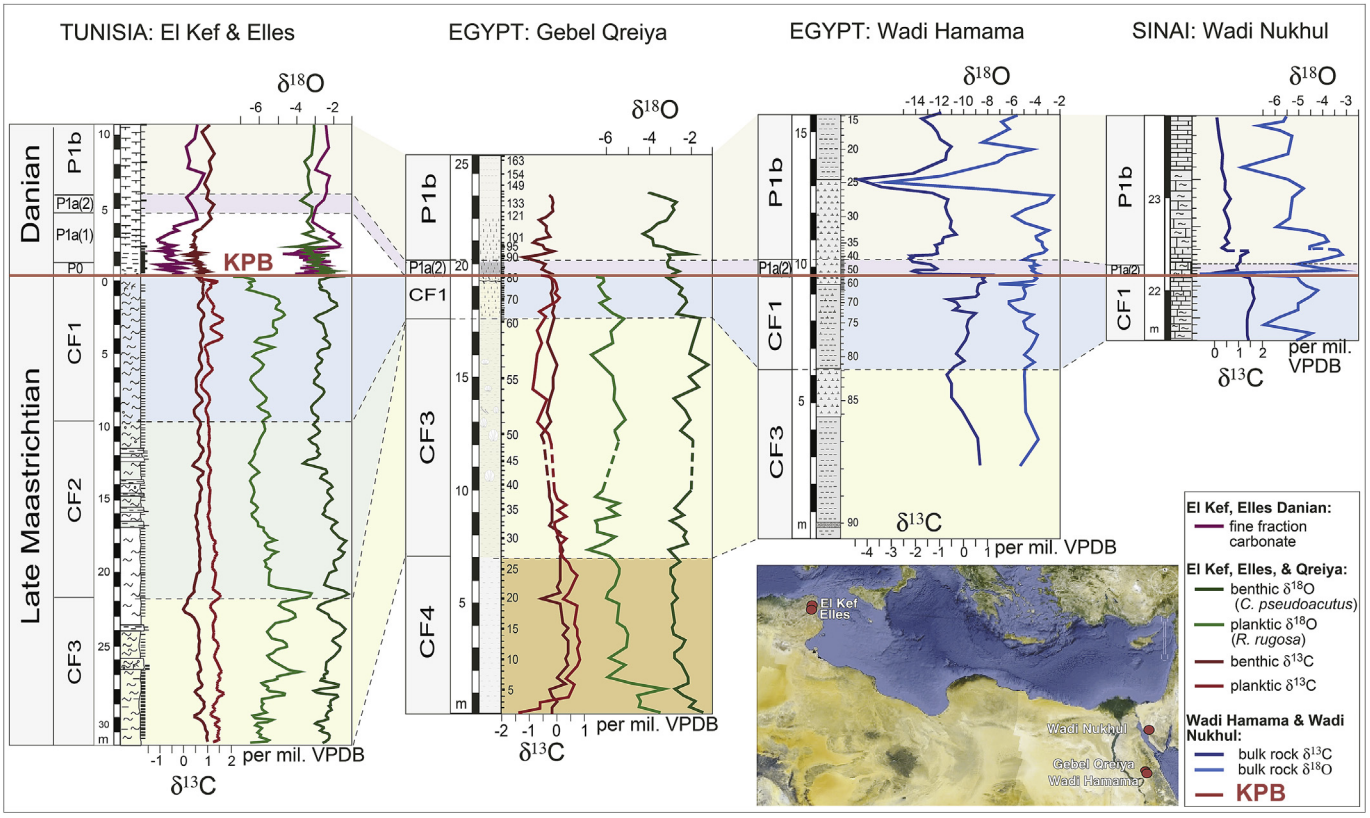

Fig. 9. Carbon and oxygen isotopes of three sections from central Egypt and Sinai compared with Elles, (Maatrichtian, Stüben et al., 2003) and El Kef, Tunisia (Danian, Keller and Lindinger, 1989). Inset shows the present day location of these sections.

lighter $\delta^{13}C$ values relative to other species (except *G. cretacea*). In central Egypt and Sinai, *P. palpebra* and *P. hariaensis* are present, but rare and the combined abundance of *P. costulata* and *P. costellifera* reaches a maximum of 25% during warm intervals (Figs. 6–8). Their low abundance indicates a less oligotrophic environment, consistent with the mesotrophic environment in the eastern Tethys (Abramovich et al., 2003, 2010).

Guembelitria blooms: high-stress environment

Among late Maastrichtian to early Danian planktic foraminifers, the tiny triserial *Guembelitria cretacea* species have the lightest $\delta^{13}C$ values indicating a habitat in the uppermost part of the ocean (Abramovich et al., 2010; Pardo and Keller, 2008). A more diverse group of *Guembelitria* morphotypes evolved in the early Danian (*G. trifolia*, *G. danica*, *G. dammula*, *G. irregularis*; Plate 4, 9–12) with

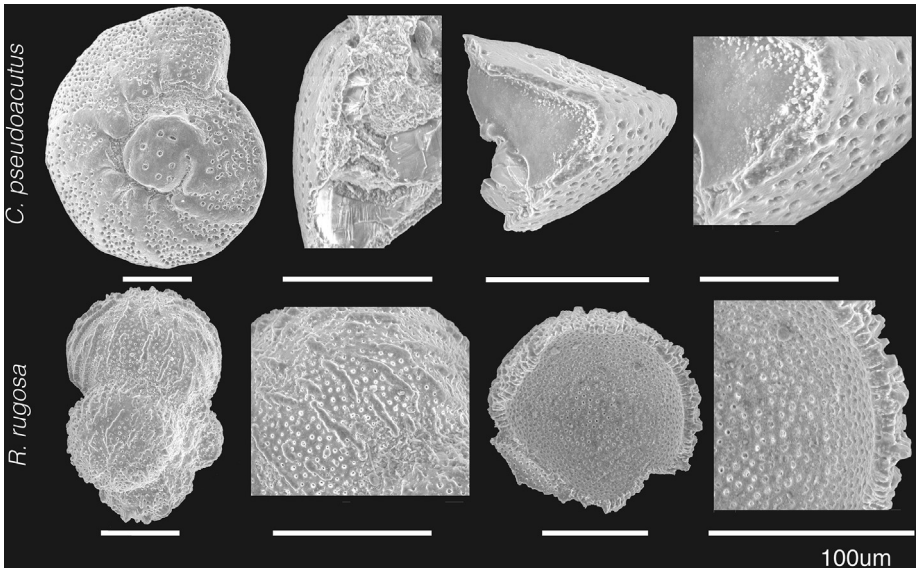

Fig. 10. Scanning electron micrograph (SEM) images of planktic (*R. rugosa*) and benthic (*C. pseudoacutus*) foraminifers analyzed for stable isotopes. Note that the relatively well-preserved planktic tests show some recrystallization and calcite overgrowth and benthic foraminiferal tests are infilled with secondary calcite.

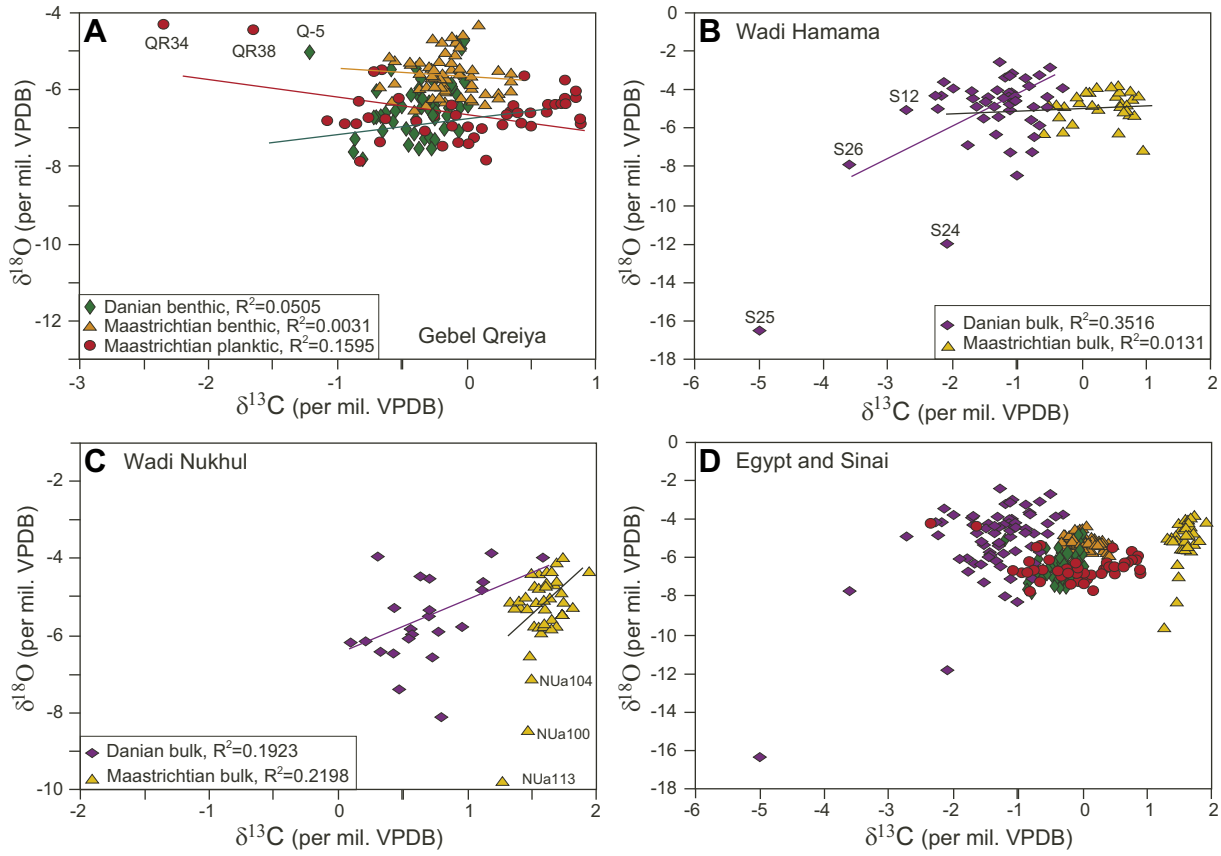

Fig. 11. $\delta^{13}C$ and $\delta^{18}O$ cross-plots for the three sites analyzed in Egypt. The generally low correlation coefficient indicates a limited degree of diagenetic alteration. Gebel Qreiya, planktic foraminiferal tests show a slightly higher R^2 value, indicating the higher susceptibility of thin planktic tests to diagenesis as compared to thick-walled benthics.

significantly ($p = 0.03$) lighter $\delta^{13}C$ values (Pardo and Keller, 2008). Among planktic foraminifers, *Guembelitria* morphotypes, especially *G. cretacea*, are unique as they erupt in great blooms during times of high environmental stress and quickly disappear when conditions return to normal. They are usually associated with mesotrophic environments such as near-shore continental shelf, upwelling areas and regions under volcanic influence (Keller and Abramovich, 2009; Keller and Pardo, 2004; Pardo and Keller, 2008). *Guembelitria cretacea* is, therefore, interpreted to have had a wider range of tolerance enabling it to survive in high-stress conditions detrimental to other species (Abramovich and Keller, 2003; Keller, 2005; Keller and Abramovich, 2009). The "blooms" strongly indicate r-selected behavior, which is a common survival strategy in unpredictable and stressful environments where quick reproduction increases the chance of survival (Pardo and Keller, 2008; Keller and Abramovich, 2009).

Guembelitria blooms were first noted in the aftermath of the KPB mass extinction and have since been observed during the late Maastrichtian and early Danian invariably in high-stress environments where few other species thrived or even survived (reviews in Keller and Pardo, 2004; Pardo and Keller, 2008; Keller and Abramovich, 2009). Abramovich et al. (2010, p. 12) suggest that the low $\delta^{13}C$ values of *Guembelitria* can be attributed to living in the uppermost part of the surface waters where photosynthesis is inhibited by high UV radiation and therefore the niche is uninhabited by other foraminifers such as symbiotic species and nutrition-deprived heterotrophs. This adaptation could explain the opportunistic *Guembelitria* blooms at times when most or all other species decrease or disappear. A return to normal, more-diverse assemblages and the end of *Guembelitria* dominance may thus indicate an abatement of crisis conditions.

At Gebel Qreiya, multiple *Guembelitria* blooms reach 60% relative abundance in zones CF4 and CF3, with maximum abundance of 80–90% at the top of CF3 below the CF3/CF1 hiatus (Fig. 12). Similar blooms are observed in CF1 at Gebel Qreiya, Wadi Hamama and Wadi Nukhul (Figs. 6–8). Each *Guembelitria* bloom correlates with a relative decrease in heterohelicid abundance as well as other mixed-layer species. In CF1, *Guembelitria* blooms reach a maximum of 50–70%, but strongly decrease during the climate warming when the biserial species dominate the assemblages. The relationship between *Guembelitria* blooms and surface productivity appears more complicated (Fig. 12). Abramovich et al. (2010) observed that *Guembelitria* blooms in CF3–CF4 and CF2–CF1 of the Negev coincide with two warming events. However, in the shallow shelf environment of Texas, *Guembelitria* blooms of CF1 show no strong correlation with low productivity, higher temperatures or freshwater influx (Abramovich et al., 2011). Similarly, no strong correlation with climate warming is observed in the Sinai and central Egypt.

The immediate post-KPB record cannot be assessed based on central Egypt, Sinai, or Negev sections because the basal Danian is missing including P0 and most of P1a. In the upper part of P1a (upper P1a(2) above the KPB hiatus), *Guembelitria* blooms rapidly decrease from 55% and reappear in P1b throughout this area (Keller and Benjamini, 1991; Keller, 2002; Keller et al., 2002, this study). In between these two early Danian *Guembelitria* blooms there is a suc1cessive dominance of small Danian species beginning with *Parvularugoglobigerina (P. eugubina*, *P. longiapertura* and *P. extensa*) followed by *Woodringina* and *Chiloguembelina*

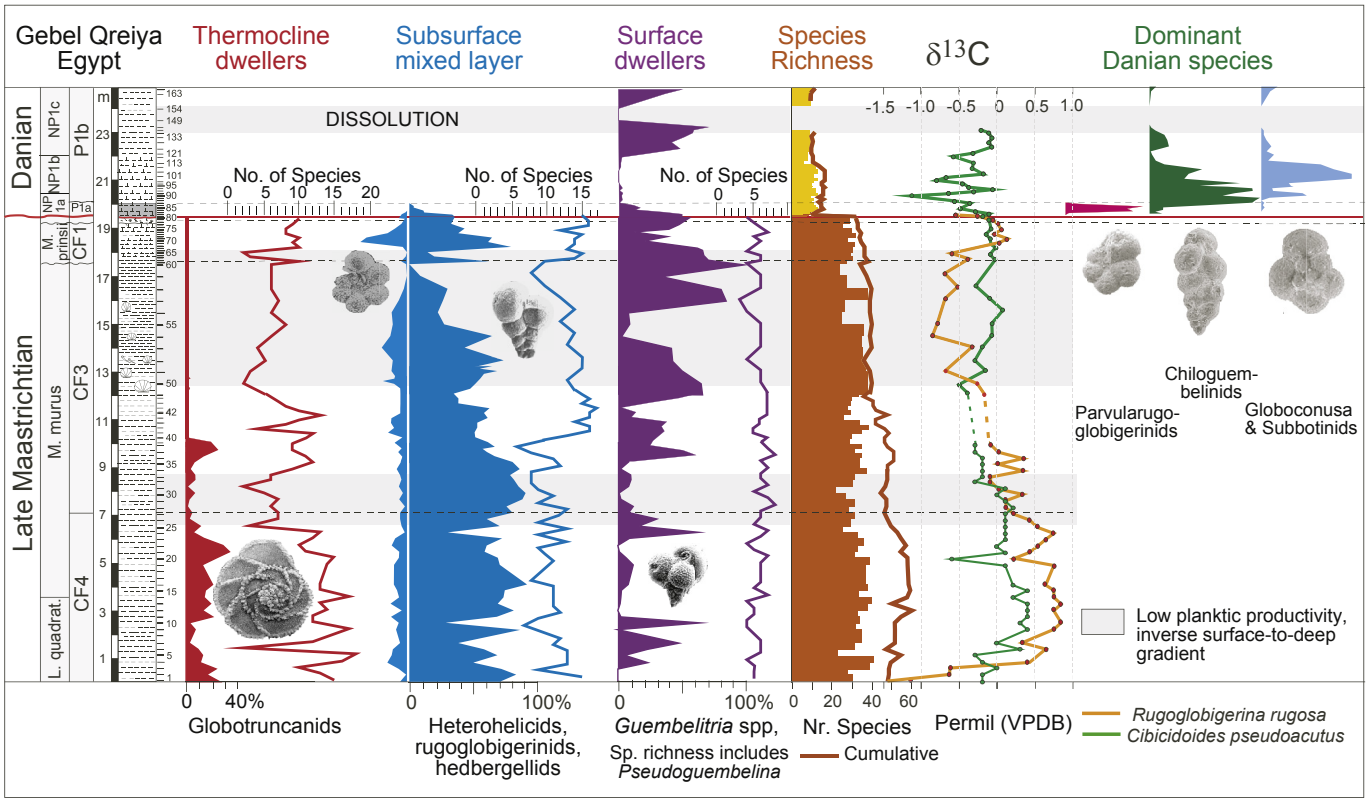

Fig. 12. Paleoenvironmental interpretation of late Maastrichtian to early Danian planktic foraminifera and stable isotopes at Gebel Qreiya. Note the strong decrease in abundance and species diversity of globotruncanids (thermocline dwellers) in CF3 well before the KPB. See text for discussion.

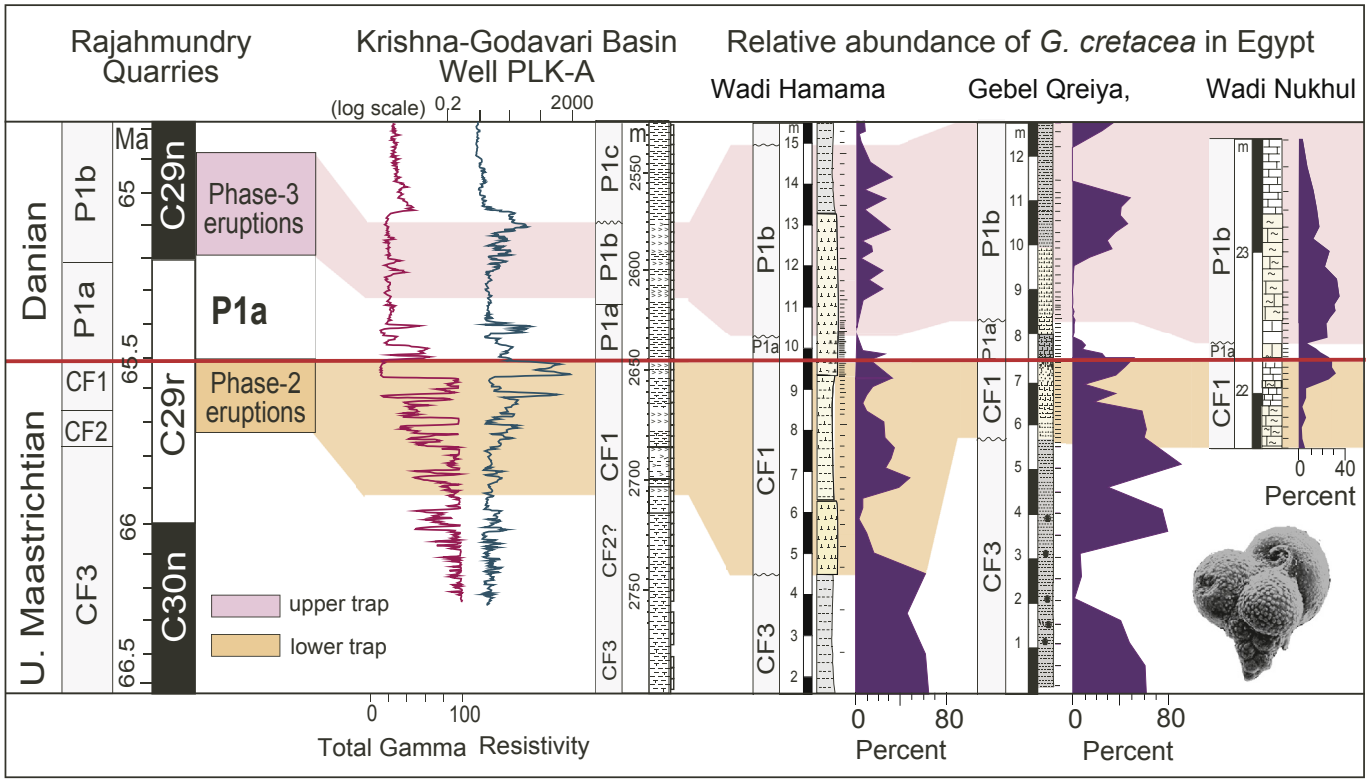

Fig. 13. Phase 2 and phase 3 Deccan volcanism and intertrappean sediments in outcrops and subsurface cores of the Krishna-Godavari Basin correlated with late Maastrichtian CF1 and early Danian P1b high-stress environments marked by *Guembelitria* blooms in Egypt.

(*W. hornerstownensis*, *W. claytonensis*, *C. morsei*, *C. midwayensis*) and ending with *Globoconusa daubjergensis* (Fig. 12). These rapid shifts in dominance suggest an unstable high-stress environment during the early post-KPB recovery phase, followed by the *Guembelitria* bloom dominated high-stress environment in P1b.

It is interesting to note that blooms of dinoflagellate *Thoracosphaera* spp. at Wadi Hamama (Fig. 9) and nannofossil *Braarudosphaera bigelowii* at Gebel Qreiya (Fig. 8, Tantawy, 2003) exist in NP1b/NP1c (C28n), which is well above planktic foraminiferal P1b (Fig. 5). There appears to be no consistent correlation of these blooms with *Guembelitria* or *G. daubjergensis* blooms, suggesting that they do not respond to the same environmental stresses. However, a good correlation was observed in the late Maastrichtian between *Guembelitria cretacea* and calcareous nannofossil blooms (*Micula decussata*, *Arkhangelskiella cymbiformis*, *Watznaueria barnesia*) associated with volcanically induced stress in the Indian Ocean (Tantawy et al., 2009).

8. *Guembelitria* blooms linked with Deccan volcanism

Late Maastrichtian Deccan phase 1 ~67.4 ± 0.6 Ma

It is tempting to link global *Guembelitria* blooms to major catastrophic events, such as the three major phases of Deccan volcanism and associated environmental and climatic consequences. The earliest Deccan eruption phase 1 (6% of the total lava pile) in C30r (~67.4 ± 0.6 Ma) is correlative with CF4 (Fig. 5). A major *Guembelitria* bloom was observed in Madagascar in CF4 (Abramovich et al., 2002), in south Atlantic DSDP Site 525 (Li and Keller, 1998a), in deep wells of the Cauvery Basin of southern India, in outcrops of the Negev and Texas (Abramovich et al., 2010, 2011; Keller et al., 2012) and now at Qreiya in central Egypt (Figs. 6 and 11). Two short-lived *Guembelitria* blooms are present at Gebel Qreiya, and the one near the CF4/CF3 boundary is associated with the disappearance of *G. bulloides*, *R. plummerae* and *R. fornicata*. This extinction event is noted not only in Egypt, but also in Madagascar (Abramovich et al., 2002) and South Atlantic Site 525 (Li and Keller, 1998a). The age of this interval correlates well with Deccan Volcanic phase 1 (67.4 Ma). There are also major *Guembelitria* blooms in CF3 at various localities, which may be linked to Deccan volcanism, or possibly Ninetyeast Ridge volcanism in the Indian Ocean, which coincides with CF3 and may have resulted in *Guembelitria* blooms and nannofossil species blooms at least regionally (Keller, 2003; Tantawy et al., 2009). These blooms may be related to major volcanism and associated climate change, increased continental weathering and drawdown of excess atmospheric CO_2.

Late Maastrichtian Deccan phase 2: C29r zone CF1

The most massive Deccan volcanic eruptions occurred during phase 2 with about 80% of the total lava pile. The world's largest (by volume) and longest lava flows erupted at this time spanning over 1000 km across India and out into the Bay of Bengal (Keller et al., 2008; Self et al., 2008). A total of four equally long lava flows were documented in deep wells of the Krishna-Godavari Basin correlative with CF1. Intertrappean sediments between these lava flows reveal the rapid and devastating species extinctions after each lava flow with the fourth lava flow ending with the mass extinction at the KT boundary (Keller et al., 2011a, 2012). In Meghalaya, NE India, 800 km from the Deccan Volcanic Province high-stress deformed *Guembelitria* blooms dominate (>95%) faunal assemblages of CF1 correlative with phase 2 Deccan volcanism (Gertsch et al., 2011). In Egypt, *Guembelitria* blooms are also observed in CF1, although this interval is incomplete due to hiatuses, and similar blooms are present in CF3 (Fig. 12). Zone CF1 *Guembelitria* blooms have been documented globally from nearshore to open marine environments from India, to Madagascar, eastern Mediterranean, Texas, Brazil, and Argentina (Abramovich et al., 2002; Keller et al., 2007, 2011b; Abramovich et al., 2010, 2011; Gertsch et al., 2013). These *Guembelitria* blooms generally coincide with the CF1 global warming, which has been linked to Deccan volcanism (Li and Keller, 1998a,b; Wilf et al., 2003; Thibault and Gardin, 2007; Abramovich et al., 2010; Keller et al., 2012).

Early Danian Deccan phase 3: C29n zone P1b

Keller and Benjamini (1991) first observed *Guembelitria* blooms in a clay layer from the early Danian P1b in the Negev coincident with a major negative $\delta^{13}C$ excursion similar to the KT boundary mass extinction (Magaritz et al., 1992). Until recently, this *Guembelitria* event remained an enigma. The discovery of planktic foraminifers in intertrappean sediments of deep wells from the Krishna-Godavari basin yielded not only age control for the KPB relative to phase 2 eruptions, but also for the early Danian phase 3. This last phase of Deccan volcanism began in the early Danian near the base of C29n correlative with P1b and *Guembelitria* blooms (Fig. 13). Phase 3 accounts for ~14% of the total Deccan Traps with four of the longest lava flows across India similar to phase 2 (Keller et al., 2012). Intertrappean sediments yield dwarfed, low-diversity planktic foraminiferal assemblages. Return to normal-sized morphologies and more diverse species assemblages occurred only after the last phase 3 lava flows. The same pattern is observed in Meghalaya, NE India, and Cauvery Basin of southern India (Keller unpublished data). Zone P1b *Guembelitria* blooms have now been documented from Egypt (Figs. 6–10), North Atlantic and Texas (Keller et al., 2011b). This suggests that the long-delayed post-KPB recovery was likely due to Deccan volcanism and that normal conditions for marine plankton only returned after the end of Deccan volcanism.

9. Conclusions

Planktic foraminiferal assemblages from the late Maastrichtian through early Paleocene reveal a series of high-stress intervals marked by *Guembelitria* blooms, low-diversity assemblages, species dwarfing and reduced abundance of keeled globotruncanids associated with low surface productivity rapid global climate warming and associated changes in the water-mass stratification. These high-stress assemblages are prominent in late Maastrichtian zones CF4–CF3, CF1 and early Danian zones P0–P1a and P1b in Egypt with predominantly global distributions. The three main Deccan eruptions closely correspond with these high-stress intervals.

1) Phase 1 in C30r (CF4) coincides with the disappearance of *G. bulloides*, *R. plummerae* and *R. fornicata* also recorded in Madagascar and South Atlantic Site 525, bracketed by two brief *Guembelitria* blooms.
2) Phase 2 in C29r (CF1) ends at the KPB mass extinction and may have been the principle contributor to the long-term climatic and environmental stresses of the late Maastrichtian leading to the KPB mass extinction.
3) Phase 3 near the C29r/C29n boundary (P1b) in the early Danian appears to be the cause for the long-delayed recovery after the mass extinction. The onset of full biotic recovery is observed in assemblages of P1c, after the cessation of phase 3 volcanism.

Acknowledgments

We are grateful to Associate Editor Peter Harries and two anonymous reviewers for their insightful comments and suggestions. The material for this study is partially based upon work supported by the US National Science Foundation through grant NSF OISE-0912144, EAR-0207407, EAR-0447171, EAR-1026271 and Princeton University's Scott and Tuttle Funds. The isotope analyses were conducted at the University of Lausanne and supported by the Egyptian Ministry of Higher Education (mission No. 001/013/104) (HK).

References

Abdel Razik, 1972. Comparative studies on the Upper Cretaceous–Early Paleogene sediments on the Red Sea coast, Nile Valley and Western Desert, Egypt. Sixth Arab Petroleum Congress, Algiers 71, pp. 1–23.

Abramovich, S., Keller, G., 2002. High stress late Maastrichtian paleoenvironment: inference from planktonic foraminifera in Tunisia. Palaeogeography, Palaeoclimatology, Palaeoecology 178, 145–164.

Abramovich, S., Keller, G., 2003. Planktonic foraminiferal response to the latest Maastrichtian abrupt warm event: a case study from South Atlantic DSDP Site 525A. Marine Micropaleontology 48 (3–4), 225–249.

Abramovich, S., Almogi-Labin, A., Benjamini, C., 1998. Decline of the Maastrichtian pelagic ecosystem based on planktic foraminifera assemblage change: Implication for the terminal Cretaceous faunal crisis. Geology 26 (1), 63–66.

Abramovich, S., Keller, G., Adatte, T., Stinnesbeck, W., Hottinger, L., 2002. Age and paleoenvironment of the Maastrichtian to Paleocene of the Mahajanga Basin, Madagascar: a multidisciplinary approach. Marine Micropaleontology 47, 17–70.

Abramovich, S., Keller, G., Stüeben, D., Berner, Z., 2003. Characterization of late Campanian and Maastrichtian planktonic foraminiferal depth habitats and vital activities based on stable isotopes. Palaeogeography, Palaeoclimatology, Palaeoecology 202 (1–2), 1–29.

Abramovich, S., Yovel-Corem, S., Almogi-Labin, A., Benjamini, C., 2010. Global climate change and planktic foraminiferal response in the Maastrichtian. Paleoceanography 25 (2), 1–15.

Abramovich, S., Keller, G., Berner, Z., Cymbalista, M., Rak, C., 2011. Maastrichtian Planktic Foraminiferal Biostratigraphy and Paleoenvironment of Brazos River, Falls County, Texas. In: Keller, G., Adatte, T. (Eds.), 100SEPM Special Publication, pp. 123–156.

Adatte, T., Keller, G., Stüeben, D., Harting, M., Kramer, U., Stinnesbeck, W., Abramovich, S., Benjamini, C., 2005. Late Maastrichtian and K/T paleoenvironment of the eastern Tethys (Israel): mineralogy, trace and platinum group elements, biostratigraphy and faunal turnovers. Bulletin de la Société Géologique de France 176 (1), 37–55.

Alvarez, W., Kauffman, E.G., Surlyk, F., Alvarez, L.W., Asaro, F., Michel, H.V., 1980. Impact Theory of Mass Extinctions and the Invertebrate Fossil Record. Advancement Of Science 223 (4641), 1135–1141.

Barrera, E., Keller, G., 1990. Foraminiferal stable isotope evidence for gradual decrease of marine productivity and Cretaceous species survivorship in the earliest Danian: Paleoceanography, 5, pp. 867–890.

Bruns, P., Rakoczy, H., Pernicka, E., Dullo, W.-C., 1997. Slow sedimentation and Ir anomaly at the Cretaceous/Tertiary boundary. Geologische Rundschau 86, 168–177.

Cande, S.C., Kent, D.V., 1995. Revised calibration of the geomagnetic polarity timescale for the Late. Journal of Geophysical Research 100, 6093–6095.

Chenet, A.-L., Quidelleur, X., Fluteau, F., Courtillot, V., Bajpai, S., 2007. $^{40}K–^{40}Ar$ dating of the Main Deccan large igneous province: Further evidence of KPB age and short duration. Earth and Planetary Science Letters 263 (1–2), 1–15.

Chenet, A.-L., Fluteau, F., Courtillot, V., Gérard, M., Subbarao, K.V., 2008. Determination of rapid Deccan eruptions across the Cretaceous-Tertiary boundary using paleomagnetic secular variation: Results from a 1200-m-thick section in the Mahabaleshwar escarpment. Journal of Geophysical Research 113 (B4).

Chenet, A.-L., Courtillot, V., Fluteau, F., Gérard, M., Quidelleur, X., Khadri, S.F.R., Subbarao, K.V., Thordarson, T., 2009. Determination of rapid Deccan eruptions across the Cretaceous-Tertiary boundary using paleomagnetic secular variation: 2. Constraints from analysis of eight new sections and synthesis for a 3500-m-thick composite section. Journal of Geophysical Research 114 (B6), 1–38.

Courtillot, V., Besse, J., Vandamme, D., Montigny, R., Jaeger, J.-J., Cappetta, H., 1986. Deccan flood basalts at the Cretaceous/Tertiary boundary? Earth and Planetary Science Letters 80 (3–4), 361–374.

Courtillot, V., Féraud, G., Maluski, H., Vandamme, D., Moreau, M.G., Besse, J., 1988. Deccan flood basalts and the Cretaceous/Tertiary boundary. Nature 333, 843–846.

Dercourt, J., Ricou, L.E., Vrielynck, B., 1993. Atlas Tethys Paleoenvironmental Maps. Gauthier-Villars, Paris, p. 307.

Donovan, A.D., Baum, G.R., Blechschmidt, G.L., Loutit, T.S., Pflum, C.E., Vail, P.R., 1988. Sequence stratigraphic setting of the Cretaceous–Tertiary Boundary in Central Alabama. In: Wilgus, C.K., Hastings, B.K., Posamentier, H., Van Wagoner, J., Ross, C.A., Kendall, C.G.St.C. (Eds.), Sea-Level Changes—An integrated Approach, SEPM Special Publication, 42, pp. 299–307.

Gertsch, B., Keller, G., Adatte, T., Garg, R., Prasad, V., Berner, Z., Fleitmann, D., 2011. Environmental effects of Deccan volcanism across the Cretaceous–Tertiary transition in Meghalaya, India. Earth and Planetary Science Letters 310 (3–4), 272–285.

Gertsch, B., Keller, G., Adatte, T., Berner, Z., 2013. The Cretaceous-Tertiary boundary (KTB) transition in NE Brazil. Journal of the Geological Society of London 170, 249–262.

Gradstein, F.M., Ogg, J.G., Smith, A.G., 2004. A geologic time scale. U.K. Cambridge University Press, Cambridge, p. 598.

Keller, G., 2001. The end-cretaceous mass extinction in the marine realm: year 2000 assessment. Planetary and Space Science 49 (8), 817–830.

Keller, G., 2002. Guembelitria-dominated late Maastrichtian planktic foraminiferal assemblages mimic early Danian in central Egypt. Marine Micropaleontology 47, 71–99.

Keller, G., 2003. Biotic effects of impacts and volcanism. Earth and Planetary Science Letters 215 (1–2), 249–264.

Keller, G., 2005. Biotic effects of late Maastrichtian mantle plume volcanism: implications for impacts and mass extinctions. Lithos 79 (3), 317–341.

Keller, G., 2011. Defining the Cretaceous–Tertiary Boundary: A PracticaL Guide and Return to First Principles. Society for Sedimentary Geology Special Volume 100, 23–42.

Keller, G., Abramovich, S., 2009. Lilliput effect in late Maastrichtian planktic foraminifera: Response to environmental stress. Palaeogeography, Palaeoclimatology, Palaeoecology 284 (1–2), 47–62.

Keller, G., Benjamini, C., 1991. Paleoenvironment of the Eastern Tethys in the Early Paleocene. Palaios 6, 439–464.

Keller, G., Lindinger, M., 1989. Stable isotope, TOC and $CaCO_3$ record across the cretaceous/tertiary boundary at El Kef, Tunisia. Science 73, 243–265.

Keller, G., Pardo, A., 2004. Disaster opportunists Guembelitrinidae: index for environmental catastrophes. Marine Micropaleontology 53 (1–2), 83–116.

Keller, G., Li, L., MacLeod, N., 1995. The Cretaceous/Tertiary boundary stratotype section at El Kef, Tunisia: How catastrophic was the mass extinction? Palaeogeography Palaeoclimatology Palaeoecology 119 (3), 221–254.

Keller, G., Barrera, E., Schmitz, B., Matsson, E., 1993. Gradual mass extinction, species survivorship, and long term environmental changes across the Cretaceous-Tertiary boundary in high latitudes. Geological Society of America Bulletin 105 (8), 979–997.

Keller, G., Adatte, T., Burns, S.J., Tantawy, A.A., 2002. High-stress paleoenvironment during the late Maastrichtian to early Paleocene in central Egypt. Palaeogeography, Palaeoclimatology, Palaeoecology 187, 35–60.

Keller, G., Stinnesbeck, W., Adatte, T., Stüben, D., 2003. Multiple impacts across the Cretaceous–Tertiary boundary. Earth-Science Reviews 62 (3), 327–363.

Keller, G., Adatte, T., Tantawy, A.A., Berner, Z., Stinnesbeck, W., Stueben, D., Leanza, H.A., 2007. High stress late Maastrichtian – early Danian palaeoenvironment in the Neuquén Basin, Argentina. Cretaceous Research 28 (6), 939–960.

Keller, G., Adatte, T., Gardin, S., Bartolini, A., Bajpai, S., 2008. Main Deccan volcanism phase ends near the K–T boundary: Evidence from the Krishna–Godavari Basin, SE India. Earth and Planetary Science Letters 268 (3–4), 293–311.

Keller, G., Adatte, T., Bajpai, S., Mohabey, D.M., Widdowson, M., Khosla, A., Sharma, R., Khosla, S.C., Gertsch, B., Fleitmann, D., Sahni, A., 2009a. K–T transition in Deccan Traps of central India marks major marine Seaway across India. Earth and Planetary Science Letters 282 (1), 10–23.

Keller, G., Abramovich, S., Berner, Z., Adatte, T., 2009b. Biotic effects of the Chicxulub impact, K–T catastrophe and sea level change in Texas. Palaeogeography, Palaeoclimatology, Palaeoecology 271 (1), 52–68.

Keller, G., Bhowmick, P.K., Upadhyay, H., Dave, A., Reddy, A.N., Jaiprakash, B.C., Adatte, T., 2011a. Deccan Volcanism Linked to the Cretaceous-Tertiary Boundary Mass Extinction: New Evidence from ONGC Wells in the Krishna-Godavari Basin. Journal of the Geological Society of India 78, 399–428.

Keller, G., Abramovich, S., Adatte, T., Berner, Z., 2011b. Biostratigraphy, Age of the Chicxulub impact, and depositional environment of the Brazos River KPB sequences. In: Keller, G., Adatte, T. (Eds.), The End-Cretaceous Mass Extinction and the Chicxulub Impact in Texas, Society for Sedimentary Geology (SEPM) Special Publication, 100, pp. 81–122.

Keller, G., Adatte, T., Bhowmick, P.K., Upadhyay, H., Dave, A., Reddy, A.N., Jaiprakash, B.C., 2012. Nature and timing of extinctions in Cretaceous-Tertiary planktic foraminifera preserved in Deccan intertrappean sediments of the Krishna–Godavari Basin, India. Earth and Planetary Science Letters 341, 211–221.

Keller, G., Khozyem, H.M., Adatte, T., Malarkodi, N., Spangenberg, J.E., Stinnesbeck, W., 2013. Chicxulub Impact Spherules in the North Atlantic and Caribbean: age constraints and Cretaceous-Tertiary boundary hiatus. Geological Magazine. http://dx.doi.org/10.1017/S0016756812001069.

Li, L., Keller, G., 1998a. Maastrichtian climate, productivity and fauna1 turnovers in planktic foraminifera in South Atlantic DSDP sites 525A and 21. Marine Micropaleontology 33, 55–86.

Li, L., Keller, G., 1998b. Abrupt deep-sea warming at the end of the Cretaceous. Geology 26, 995–998.

Luger, P., 1988. Maastrichtian to Paleoocene facies evolution and the Cretaceous-Tertiary boundary in Middle and Southern Egypt. Revista española de paleontología 1, 83–90.

Magaritz, M., Benjamini, C., Keller, G., Moshkovitz, S., 1992. Early diageneitc isotopic signal at the Cretaceous/Tertiary boundary, Israel. Palaeogeography, Palaeoclimatology, Palaeoecology 91 (3), 291–304.

McLean, D., 1985. Deccan traps mantle degassing in the terminal Cretaceous marine extinctions. Cretaceous Research 6 (3), 235–259.

Miller, K.G., Sherrell, R.M., Browning, J.V., Field, M.P., Gallagher, W., Olsson, R.K., Sugarman, P.J., Tuorto, S., Wahyudi, H., 2010. Relationship between mass extinction and iridium across the Cretaceous-Paleogene boundary in New Jersey. Geology 38 (10), 867–870.

Molina, E., Alegret, L., Arenillas, I., Arz, J., Gallala, N., Hardenbol, J., von Salis, K., Steurbaut, E., Vanhenberghe, N., Zaghbib-Turki, D., 2006. The Global Boundary Stratotype Section and Point for the base of the Danian Stage (Paleocene, Paleogene, "Tertiary", Cenozoic) at El Kef, Tunisia -Original definition and revision. Episodes 29 (4), 263–273.

Nederbragt, A.J., 1991. Late Cretaceous biostratigraphy and development of Heterohelicidae (planktic foraminifera). Micropaleontology 37, 329–372.

Nordt, L., Atchley, S., Dworkin, S., 2003. Terrestrial evidence for two greenhouse events in the latest Cretaceous. GSA Today 13 (12), 4–9.

Olsson, R.K., Hemleben, C., Berggren, W.A., Huber, B.T., 1999. Atlas of Paleocene Planktonic Foraminifera. Smithsonian Contribution to Paleobiology No. 85. Smithsonian Institution Press, Washington D.C., p. 252

Pardo, A., Keller, G., 2008. Biotic effects of environmental catastrophes at the end of the Cretaceous and early Tertiary: Guembelitria and Heterohelix blooms. Cretaceous Research 29 (5–6), 1058–1073.

Pearson, P.N., Ditchfield, P.W., Singano, J., Harcourt-Brown, K.G., Nicholas, C.J., Olsson, R.K., Shackleton, N.J., Hall, M.A., 2001. Warm tropical sea surface temperatures in the Late Cretaceous and Eocene epochs. Nature 413 (6855), 481–487.

Punekar, J., Mateo, P., Keller, G., 2014. Environmental and biological effects of Deccan volcanism: A global survey. in press.

Quillévéré, F., Norris, R.D., Kroon, D., Wilson, P.A., 2008. Transient ocean warming and shifts in carbon reservoirs during the early Danian. Earth and Planetary Science Letters 265 (3), 600–615.

Robaszynski, F., Caron, M., Gonzales Donoso, J.M., Wonders, A.A.H., 1983–84. Atlas of Late Cretaceous Globotruncanids. Revue de Micropaléontologie 26, 145–305.

Said, R., 1961. Tectonic framework of Egypt and its influence on distribution of foraminifera. AAPG Bulletin 45 (2), 198–218.

Schrag, D.P., Depaolo, D.J., Richter, F.M., 1995. Reconstructing past sea surface temperatures: Correcting for diagenesis of bulk marine carbonate. Geochemica et Cosmochimica Acta 59 (11), 2265–2278.

Schulte, P., Alegret, L., Arenillas, I., Arz, J.A., Barton, P.J., Bown, P.R., Bralower, T.J., Christeson, G.L., Claeys, P., Cockell, C.S., Collins, G.S., Deutsch, A., Goldin, T.J., Goto, K., Grajales-Nishimura, J.M., Grieve, R.A.F., Gulick, S.P.S., Johnson, K.R., Kiessling, W., Koeberl, C., Kring, D.A., MacLeod, K.G., Matsui, T., Melosh, J., Montanari, A., Morgan, J.V., Neal, C.R., Norris, R.D., Pierazzo, E., Ravizza, G., Rebolledo-Vieyra, M., Reimold, W.U., Robin, E., Salge, T., Speijer, R.P., Sweet, A.R., Urrutia-Fucugauchi, J., Vajda, V., Whalen, M.T., Willumsen, P.S., 2010. The Chicxulub asteroid impact and mass extinction at the Cretaceous-Paleogene boundary. Science 327 (5970), 1214–1218.

Self, S., Thordarson, T., Widdowson, M., 2005. Gas Fluxes from Flood Basalt Eruptions. Elements 1 (5), 283–287.

Self, S., Blake, S., Sharma, K., Widdowson, M., Sephton, S., 2008. Sulfur and chlorine in late Cretaceous Deccan magmas and eruptive gas release. Science 319 (5870), 1654–1657.

Soliman, M., Habib, M., Ahmed, E., 1986. Sedimentologic and tectonic evolution of the Upper Cretaceous-Lower Tertiary succession at Wadi Qena, Egypt. Sedimentary Geology 46, 11–133.

Stüben, D., Kramar, U., Berner, Z.A., 2003. Late Maastrichtian Paleoclimatic and Paleoceanographic Changes Inferred from Sr/Ca Ratio and Stable Isotopes. Palaeogeography, Palaeoclimatology, Palaeoecology 199, 107–127.

Tantawy, A.A., 2003. Calcareous nannofossil biostratigraphy and paleoecology of the Cretaceous/Tertiary transition in the central eastern desert of Egypt. Marine Micropaleontology 47, 323–356.

Tantawy, A.A., Keller, G., Pardo, A., 2009. Late Maastrichtian volcanism in the Indian Ocean: Effects on calcareous nannofossils and planktic foraminifera. Palaeogeography, Palaeoclimatology, Palaeoecology 284, 63–87.

Thibault, N., Gardin, S., 2007. The late Maastrichtian nannofossil record of climate change in the South Atlantic DSDP Hole 525A. Marine Micropaleontology 65 (3), 163–184.

Wilf, P., Johnson, K.R., Huber, B.T., 2003. Correlated terrestrial and marine evidence for global climate changes before mass extinction at the Cretaceous–Paleogene boundary. Proceedings of the National Academy of Sciences, USA 100 (2), 599–604.